SOME ASPECTS OF THE DESIGN AND PERFORMANCE OF THE GLOBAL ECMWF SPECTRAL MODEL

A.J. Simmons
European Centre for Medium-range Weather Forecasts
Reading, United Kingdom

1. INTRODUCTION

A global spectral model with T63 truncation was introduced into operational forecasting at ECMWF in April 1983 (Simmons and Jarraud, 1984). Two years later, the horizontal resolution was increased to T106 (Jarraud et al., 1985). During the development of these two version of the model, attention has been paid to a number of aspects of the time-stepping, and to a comprehensive comparison of the sensitivity of medium-range forecasts to horizontal resolution, with forecasts carried out at truncations T21, T42, T63 and T106. Further comparisons of T63 and T106 have subsequently been carried out, and a limited number of experiments with T159 resolution has also been performed.

In this paper an account is given of the above work. The following sections 2.1 to 2.4 describe the time-stepping aspects, and the resolution experiments are discussed in sections 3.1 to 3.3. Section 4 contains some concluding remarks.

2. TIME-STEPPING ALGORITHMS FOR THE SPECTRAL MODEL

2.1 Semi-implicit treatment of vorticity and moisture advection

Robert (1981) pointed out that the timestep limit in a conventional model with semi-implicit treatment of gravity-wave terms is generally determined by the stability of the scheme for the horizontal advection of vorticity (and, by implication, the horizontal advection of moisture). This has been exploited to enable use of longer timesteps by treating semi-implictly the advection of vorticity and moisture, linearizing about advection by a zonally-uniform zonal wind. Specifically,

$$\frac{1}{2\Delta t}\left\{X(t+\Delta t) - X(t-\Delta t)\right\} = X_T - \frac{u_o}{a\cos\theta}\frac{\partial}{\partial\lambda}\left\{X(t-\Delta t) + X(t+\Delta t) - 2X(t)\right\}$$

where X_T is the explicit tendency of X, X being either the vorticity or the humidity variable, u_o is a height- and latitudinally-varying reference zonal wind, θ is latitude, λ is longitude, t is time and a is the radius of the earth. This equation is easily and cheaply solved for $X(t+\Delta t)$ in Fourier

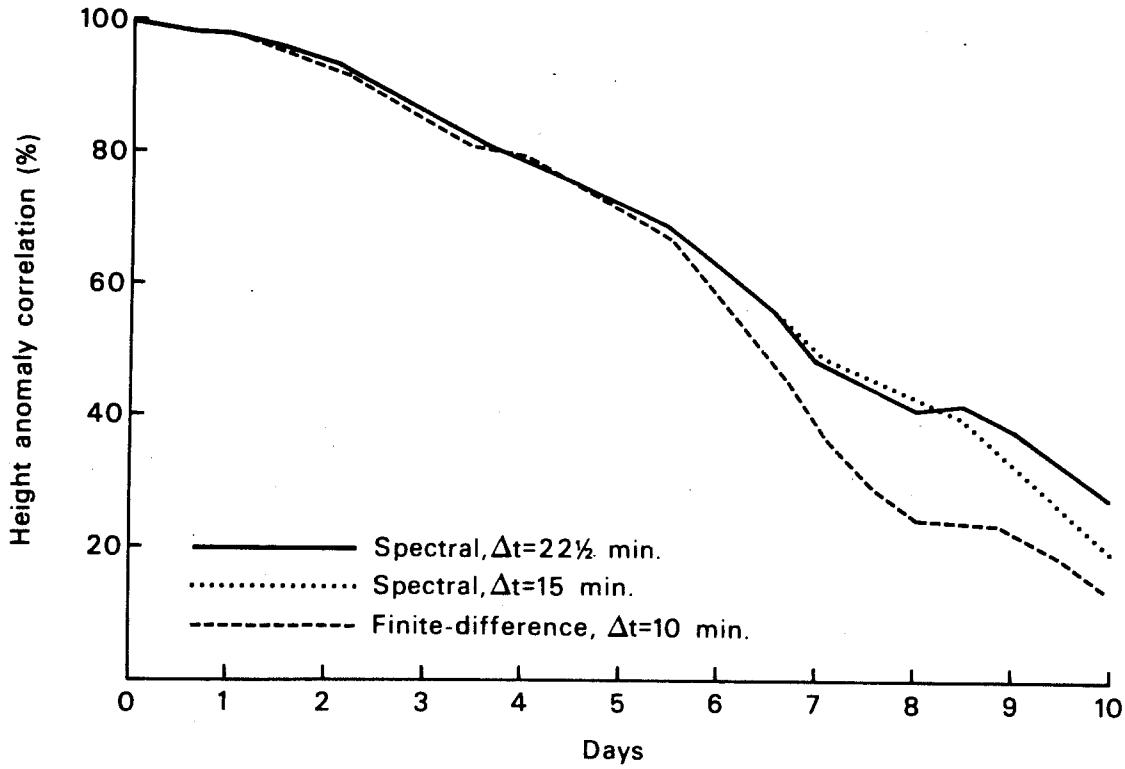

Fig. 1 Height anomaly correlations (%), calculated for the area from 20°N to 82.5°N using standard pressure levels from 1000 to 200 mb, plotted as functions of the forecast range in days. Results are shown for three forecasts (as labelled in the figure) from 4 October 1982.

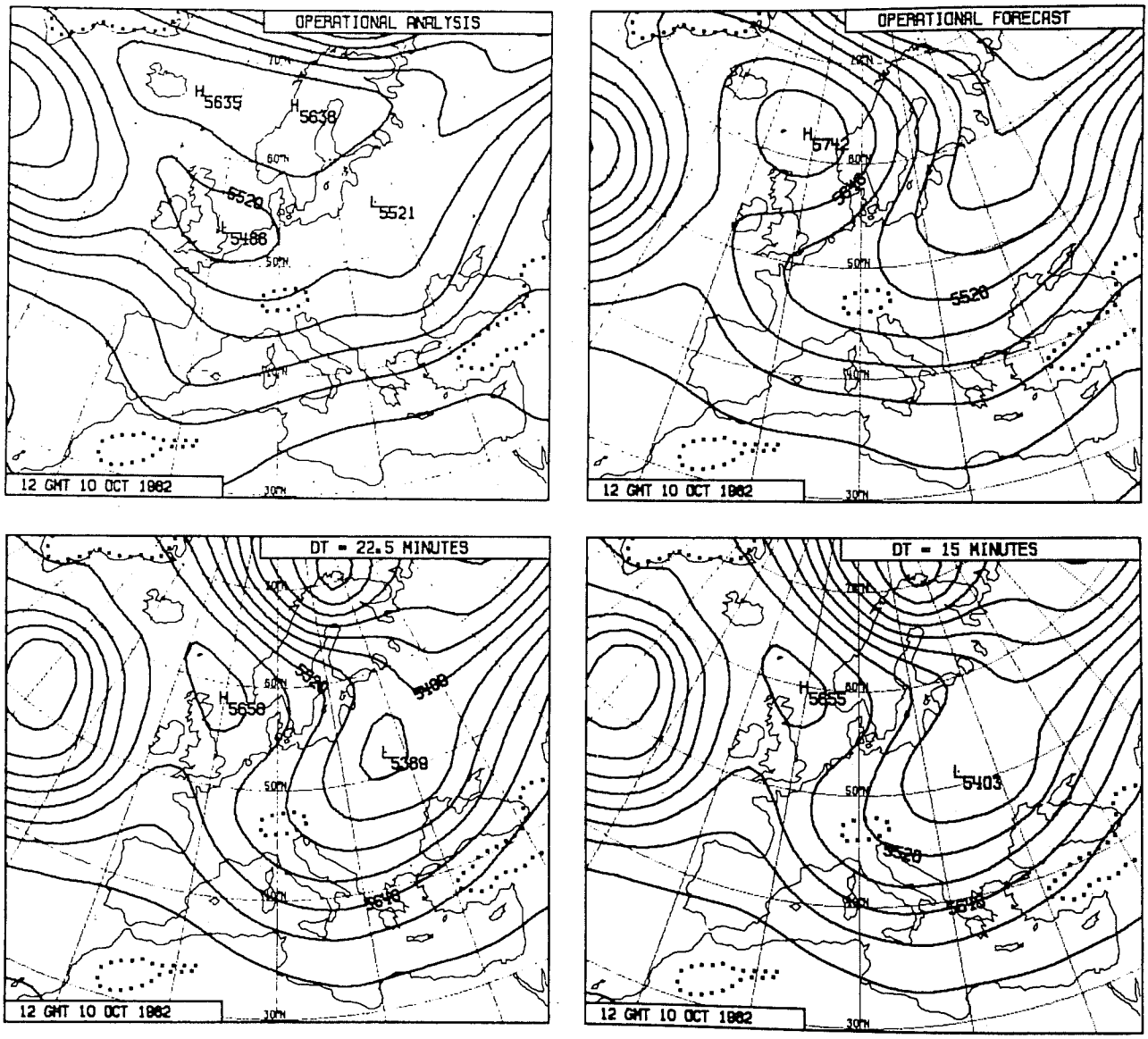

Fig. 2 Maps of 500 mb height (contour interval 60m) over Europe. The operational analysis for 10 October 1982 is shown in the upper-left panel and the 6-day operational (grid-point) forecast from 4 October carried out with a 10-minute timestep is upper right. Forecasts using the new model are shown for timesteps of 22½ minutes (new time scheme, lower left) and 15 minutes (standard time scheme, lower right).

space, although the use of integration by parts to compute spectral tendencies of vorticity necessitates the computation of values of $\partial u_o / \partial \theta$ as well as u_o for each latitude and model level. For the test reported here and for the initial operational implementation, u_o was taken to be the zonal-mean of the instantaneous model zonal wind. It was subsequently changed to be the arithmetic mean of the maximum and minimum zonal wind for timestep $t-\Delta t$, this having been found to give a slight increase in computational stability.

The scheme has, by itself, made it possible to use timesteps between 25 and 50% longer than possible with the conventional semi-implicit treatment of gravity-wave terms alone. Fig. 1 shows an objective verification of forecasts for the extratropical Northern Hemisphere for an extreme case in which strong flow in the polar stratosphere of the Southern Hemisphere resulted in the then operational 15-level grid-point sigma-coordinate model having to use a timestep of 10 minutes rather than its usual value of 15 minutes. For this example, use of a hybrid coordinate (Simmons and Burridge, 1981) reduced the strongest winds in the model stratosphere over Antarctica, since the top hybrid model level did not rise up over high ground. Thus with this coordinate a timestep of 12 minutes was possible with the grid-point model, and 15 minutes was possible with the T63 spectral model using a conventional semi-implicit scheme. Including the semi-implicit treatment of vorticity and moisture advection, a stable integration could be carried out using a timestep of 22.5 minutes, and Fig. 1 is an example of how no significant decrease in the objectively-measured forecast accuracy occurred as a result.

Fig. 2 shows corresponding maps of 500 mb height for day 6 over Europe, and it can be seen that differences between the two forecasts performed with the spectral model and different timesteps are quite negligible when compared with differences either between the spectral and operational (grid-point) forecasts, or between any of the forecasts and the analyzed state of the atmosphere. Similar conclusions were drawn from examination of three other cases prior to the operational implementation of the spectral model (Simmons and Jarraud, 1984), although a timestep as long as 22.5 minutes could not be used routinely with T63 resolution. Rather, a timestep of 20 minutes was mostly used, reduced to 18 minutes for two spells following the operational occurrence of computational instability.

2.2 Enhanced horizontal diffusion to enable use of longer timesteps

Experience with the operational forecasting system prior to May 1985 revealed two situations which limited the timestep possible in the model, even with the semi-implicit treatment of vorticity and humidity advection. The first was the occurrence of a strong polar-night jet in the stratosphere during late winter in the Southern Hemisphere. The second was a strong tropospheric jet stream over the Western Pacific during the Northern Hemisphere winter. Since May 1985 the operational (T106) model has adopted a selective enhancement of horizontal diffusion to allow use of a longer timestep than would otherwise be possible in such situations. Two types of enhancement have been employed.

The basic formulation of horizontal diffusion in the model is a simple linear 4th-order diffusion applied along the hybrid coordinate surfaces: the diffusive tendency of a variable X is of the form $- K \nabla^4 X$, where X represents vorticity, divergence, specific humidity, or temperature modified by a term proportional to $\ell n p_s$. Specification and discussion of the latter, which is chosen to reduce mixing of the temperature along sloping coordinate surfaces, is given by Simmons (1987). The diffusion coefficient K has been chosen on the basis of experimentation to be 2×10^{15} m^4 s^{-1} for T63 resolution and 10^{15} m^4 s^{-1} for T106. The use of larger coefficients for the divergence field is discussed in section 2.3

The first of the enhancements referred to above is concerned with the stability of the stratospheric flow, and entails a general substantial increase in horizontal diffusion for the smallest scales at upper model levels. For each level k, a critical total wavenumber n_k is defined. The standard diffusion coefficient K is then used for $n \leq n_k$, while for $n > n_k$ the value $K h^c$ is used, where c is the number of levels (below and including k) for which the level number, ℓ, is such that both $\ell \geq k$ and $n_\ell < n$.
Operationally h = 10 and

n_k = 83, 84, 86, 88, 90, 93, 96, 100, 103, 105, 106, ... 106 for
k = 1, 2, 3, 4, 5, 6, 7, 8, 9, 10, 11, ... 19.

This effectively acts as a reduction in model resolution at stratospheric, and to a small extent upper tropospheric, levels, without generating the noise found in earlier tests in which the highest-wavenumber components were simply set to zero at these levels.

The second approach is introduced to ensure stability for strong tropospheric flow, and involves increasing damping at levels where the maximum wind exceeds a critical value. For a particular model level, spectral components whose total wavenumber exceeds a critical value n_{crit} (which depends on the maximum windspeed computed at that level at the timestep in question) are damped by a factor

$$1 + \alpha \frac{\Delta t}{a} [\mathrm{Max}\{|\underset{\sim}{u}|\}](n-n_{crit})$$

where

$$n_{crit} = \beta/\mathrm{Max}\{|\underset{\sim}{u}|\}$$

Values $\alpha \geq 2$ and $\beta = a/\Delta t$ are sufficient to avoid exponential computational instability for the linear advection equation for a wave of scale a/n and advecting velocity $\mathrm{Max}\{|\underset{\sim}{u}|\}$. In the model, β is defined through a critical velocity, V_{crit}:

$$\beta = V_{crit} \frac{\Delta t_o n_o}{\Delta t}$$

where $\Delta t_o = 1200$s and $n_o = 63$. Here V_{crit} corresponds to a critical velocity for stability (with α=0) for a model resolution with Max $\{n\}$=63 and a 20 minute timestep. Operationally, $\alpha = 2.5$ and $V_{crit} = 85$ m s^{-1}, the latter giving $\beta = 1.009\ a/\Delta t$.

The two approaches outlined above have been used routinely to produce T106 forecasts with a 15 minute timestep, and no case of computational instability has occurred in over two years of daily use. A timestep of no more than 10 minutes would otherwise have been needed. With the 15 minute timestep the flow-dependent enhancement of diffusion takes place at levels where the maximum flow speed exceeds 63 ms^{-1}; for a level with a 100 ms^{-1} wind maximum, enhanced damping is applied to wavenumbers greater than 66.

The increase in timestep from 10 to 15 minutes is achieved at minimal computational expense, and has no apparent detrimental effect on forecast quality. To illustrate this in terms of objective verification, Fig. 3 shows anomaly correlations of 500 mb height for the extratropical Northern Hemisphere averaged over 8 10-day forecasts. One of the cases (with initial date 13 January 1985) was deliberately chosen because of the presence of a

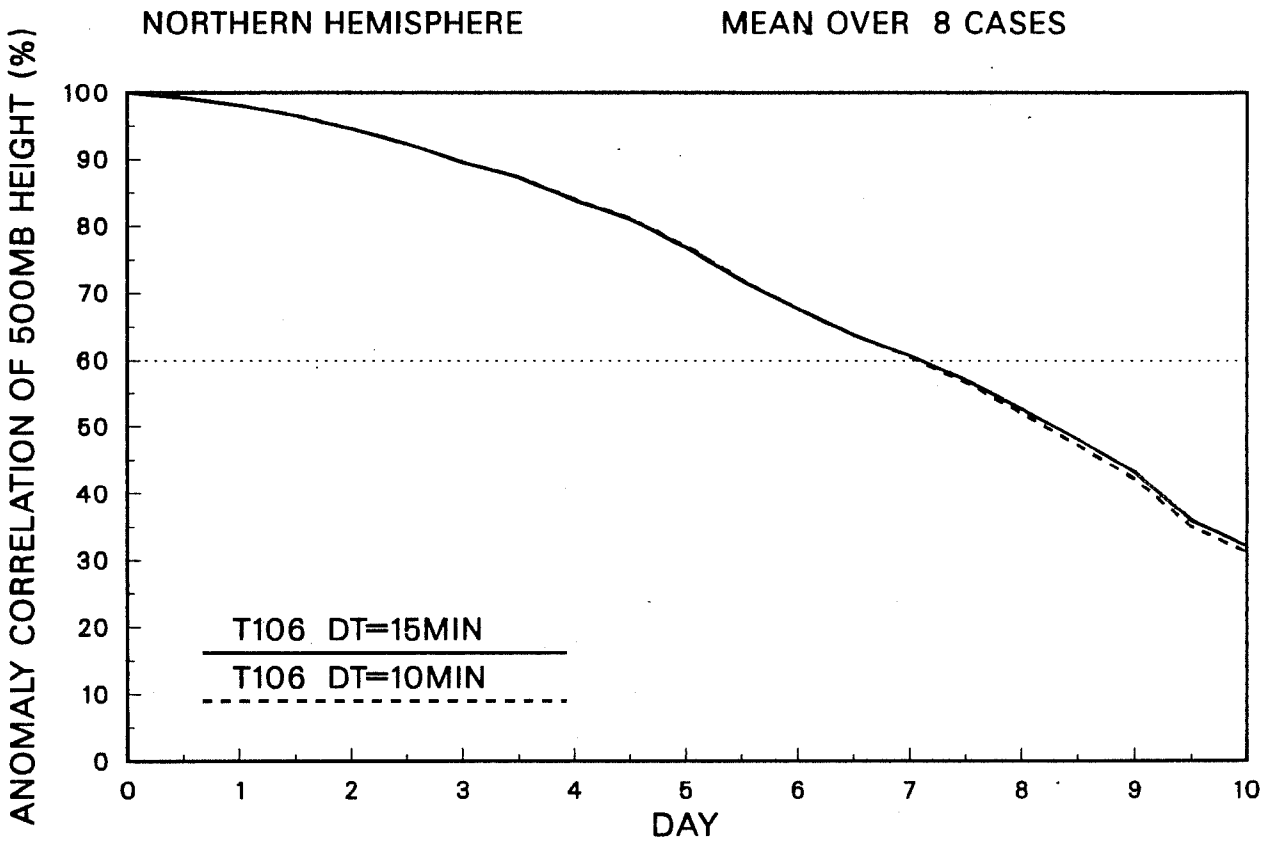

Fig. 3 Anomaly correlations (%) of 500 mb height calculated for the extratropical Northern Hemisphere, plotted as functions of the forecast range in days. Results are shown for two means of 8 T106 forecasts (as labelled).

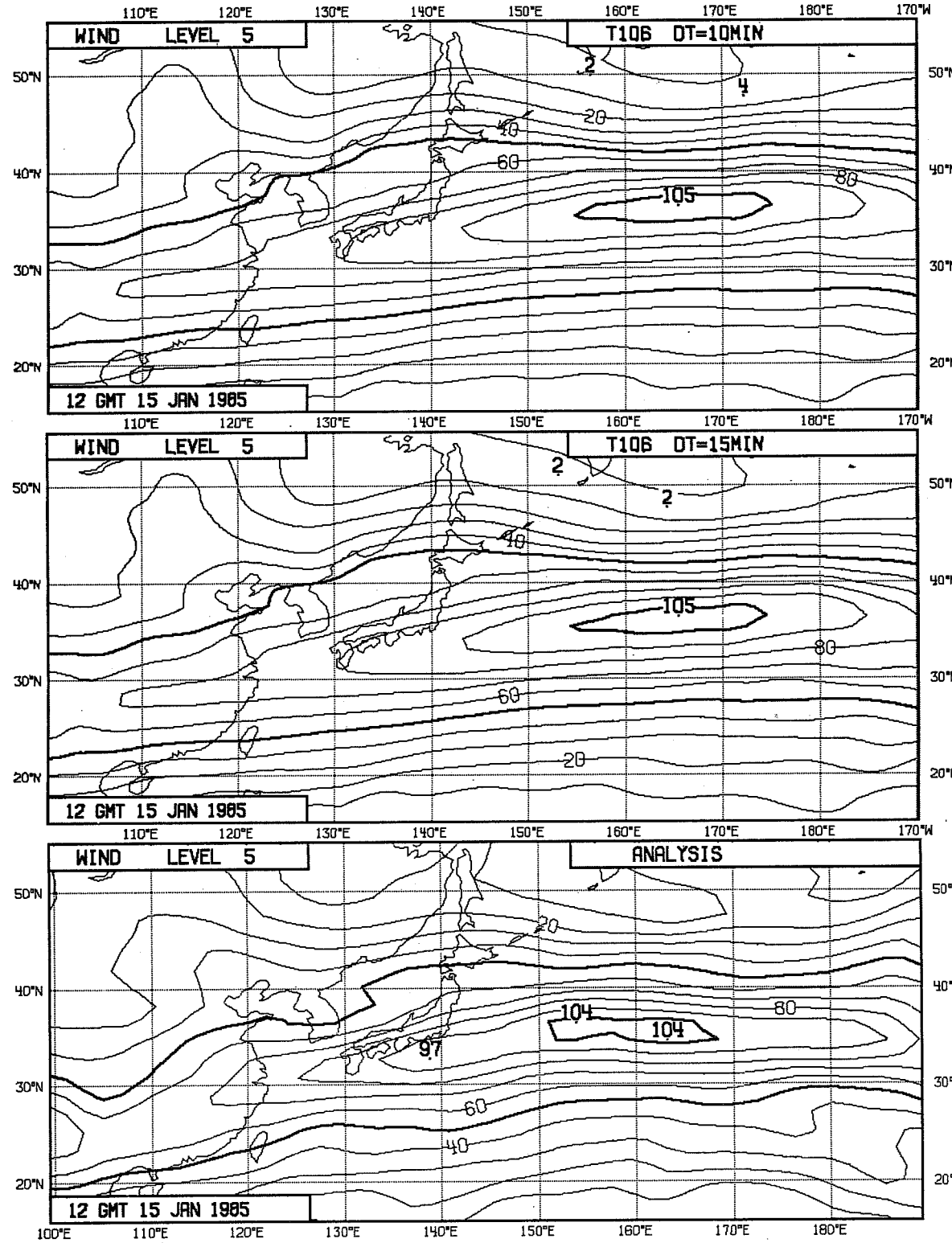

Fig. 4 Isotachs (contour interval 10 ms^{-1}) at level 5 of the 16-level model (approximately 250 mb)
Upper panel: T106 two day forecast with a 10 minute timestep
Middle panel: T106 " " " " " 15 " "
Lower panel: Verifying analysis

strong tropospheric jet stream over the Western Pacific, with maximum winds over 100 ms^{-1} during the first two days of the forecast. The others were chosen without regard to the synoptic situation, with four (Northern Hemisphere) summer cases and three more winter cases. Fig. 3 shows results obtained using a 15 minute timestep with selectively enhanced diffusion and a 10 minute timestep with no enhancement of diffusion. Both sets of forecasts were carried out using the semi-implicit treatment of vorticity and humidity advection discussed in the preceding section.

Over much of the forecast range the two curves shown in Fig. 3 are almost indistinguishable. Only beyond day 7 can a difference be seen, but this is small enough to be of no obvious significance, and the difference such as it is in fact favours the use of the longer timestep. A very similar result is found for other fields, and from verification of the forecasts for the extratropical Southern Hemisphere. Tropical wind scores also show very little difference, although they come out fractionally in favour of the shorter timestep. Synoptic assessment also shows a negligible impact of the increase in timestep.

It is important to note that the increase in timestep possible with the enhanced diffusion is not achieved at the expense of a significant reduction in jet speed. Two-day forecasts of the flow at level 5 of the 16-level model (approximately 250 mb) are shown in Fig. 4 together with the verifying analysis in the 13 January 1985 case. Despite a maximum wind persistently in excess of 100 ms^{-1} early in the forecast range, differences between 10- and 15-minute forecasts are slight.

Timesteps longer than 15 minutes are possible for T106 resolution, but indications of a deterioration in forecast quality are found. In particular, a set of 6 10-day forecasts has been carried out with a timestep of $22\frac{1}{2}$ minutes. The cases were chosen from among 24 comprising the 1st and 15th of each month for the year from May 1986 to April 1987. T63 forecasts were available for comparison with the operational T106 forecasts for the 24 cases, and the 6 cases considered here were chosen on the basis of one per two months, selecting out of the four available for each period the case which gave the largest difference between T63 and T106.

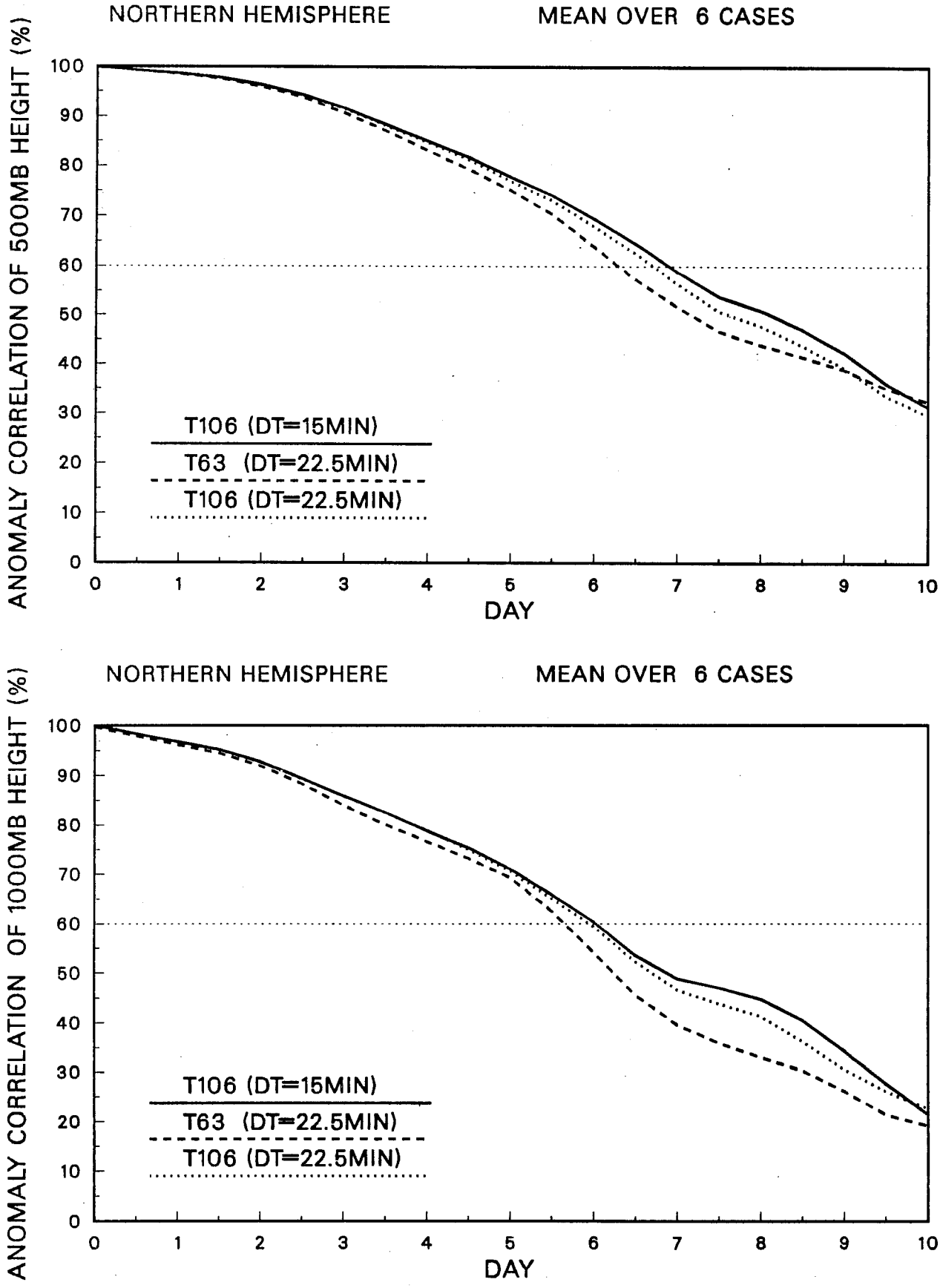

Fig. 5 Height anomaly correlations (%) for 500 mb (upper panel) and 1000 mb (lower panel) calculated for the extratropical Northern Hemisphere, plotted as functions of the forecast range. Results shown are for three means of 6 forecasts (as labelled).

Fig. 5 shows mean anomaly correlations of 500 and 1000 mb height for T106 forecasts using 15 and 22½ minute timesteps, and for the corresponding T63 forecasts, which also used a timestep of 22½ minutes. It is clear that for the first 3 to 4 days of the forecast the differences in skill between the two T106 forecasts are very small, and certainly much less than the differences between T63 and T106. However, further into the forecast range the 22½ minute T106 forecasts exhibit a poorer accuracy than the 15-minute forecasts, more so at 500 than at 1000 mb. A similar result has been found (for a different, and larger, sample of cases) comparing T63 forecasts with 15 and 22½ minute timesteps. Reducing the timestep below 22½ minutes but keeping the enhanced diffusion shows that much of the deterioration is due to the increased diffusion, rather than to the use of the longer timestep.

The similarity between the results of using 15- and 22½-minute timesteps seen in Fig. 5 for the first part of the forecast range might suggest that the larger timestep be adopted if the model were to be used for prediction out to 3 or 4 days ahead. This timestep is around a factor of 2½ to 3 larger than possible in a conventional spectral model with no semi-implicit treatment of advection and no use of enhanced diffusion. However, some cautionary remarks must be added. Firstly, objective scores for the tropics show some deterioration of the 850 mb wind field earlier in the range when using the 22½ minute timestep. Furthermore, problems concerning the computational stability of the semi-implicit treatment of gravity-wave terms (discussed in the following section) and of the time-stepping in the parametrization of low-level vertical diffusion (discussed in 2.4) may come more to the fore. In addition, all tests reported here have been for the hybrid vertical coordinate. Use of enhanced diffusion may be less satisfactory in a sigma-coordinate model, in which there are more prominent small-scale variations in upper model-level fields resulting from the small-scale variations in the height of coordinate surfaces following the model orography.

2.3 Stability of the semi-implicit gravity-wave scheme

The first year of operational forecasting with the spectral model revealed occasional cases in which noise developed along the axes of strong jet streams. The problem was particularly evident in data assimilation cycles and short-range forecasts, and in one case it was so severe that a complete computational instability of the model occurred during the 6-hour forecast of

a data assimilation cycle. Non-linear normal-mode initialization exacerbated the problem; the iteration process in the initialization tended to diverge once the noise in the 6-hour forecast had passed a critical amplitude.

Experimentation pointed to the stability of the semi-implicit time scheme for gravity-wave terms as the source of the problem. A gradual reduction in noise was found as the timestep was gradually reduced. Contrary to expectations based on the stability analysis presented by Simmons et al. (1978), reducing the value of the isothermal reference temperature used in the semi-implicit scheme reduced the noise at the jet-stream level, although in agreement with the earlier analysis, instability eventually arose elsewhere in the model atmosphere. Generation of noise was reduced when the semi-implicit scheme was modified as described below, and increasing horizontal diffusion on the divergence field alone was sufficient to prevent noise developing.

The above investigations led to the following model changes:

(i) The operator $(\bar{})$ that appears in a conventional semi-implicit scheme:

$$\bar{X} = 0.5(X(t+\Delta t) + X(t-\Delta t))$$

was changed to

$$\bar{X} = 0.25X(t) + 0.375(X(t+\Delta t) + X(t-\Delta t))$$

This reduces the slowing of gravity waves by the scheme, and a stability analysis of the type reported by Simmons et al. (1978) and Simmons and Burridge (1981) indicates a computational stability only marginally less than that of the conventional scheme. Further details are given in the appendix.

(ii) Horizontal diffusion of divergence was carried out after the $(t+\Delta t)$ value was used to update the temperature and surface pressure fields, rather than before as hitherto.

(iii) The coefficient of horizontal diffusion of the divergence field was increased by a factor of 10.

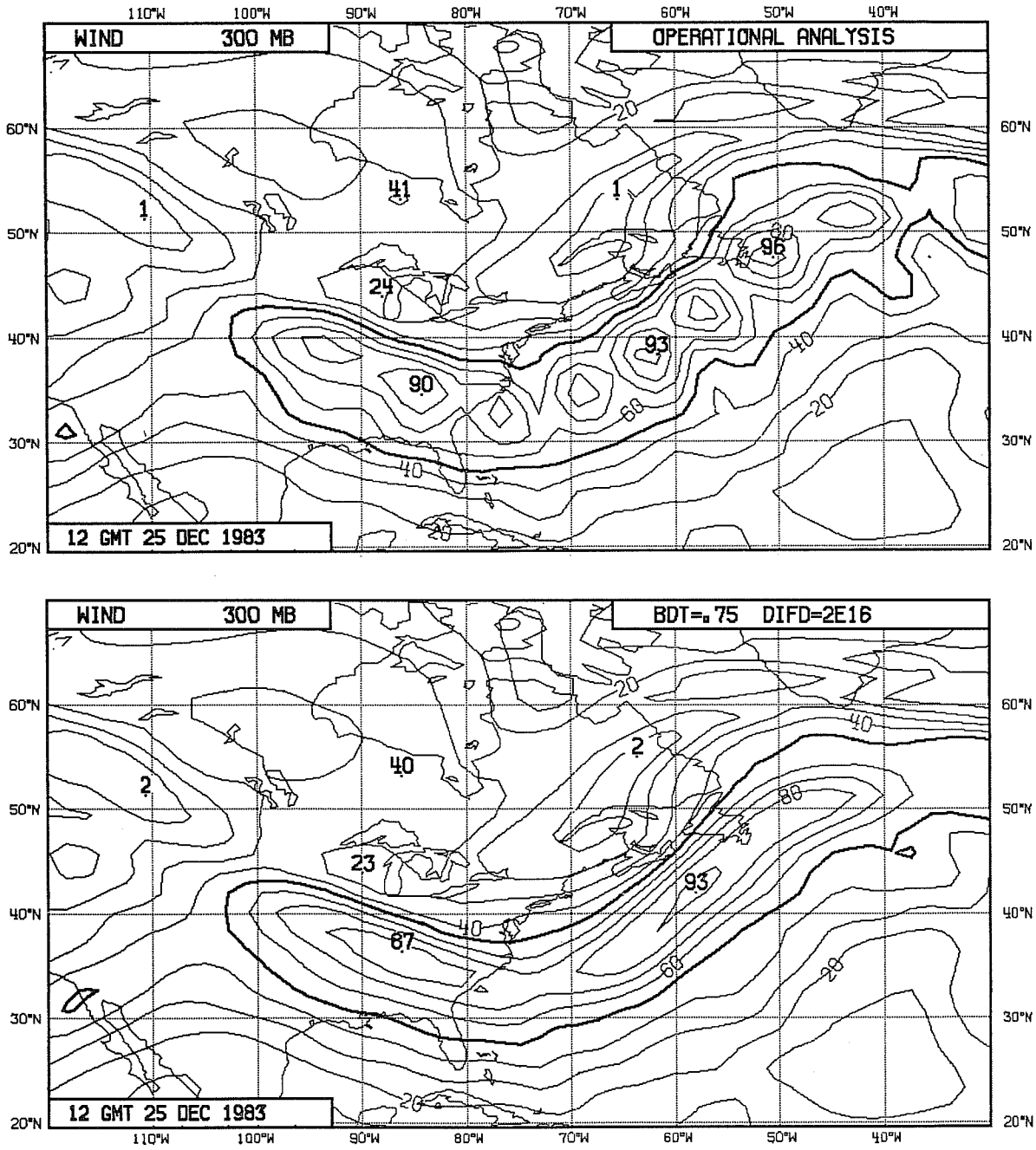

Fig. 6 Influence of the formulation for the assimilating models on the analyses of the 300 mb wind speed over Eastern North America and the North-West Atlantic for 12 GMT 25 December 1983.
Upper panel: Operational analysis.
Lower panel: Analysis with assimilating model modified as specified in the text.

To illustrate the impact of these changes, Fig. 6 presents analyses of the 300 mb wind speed over Eastern North America and the North-West Atlantic for Christmas Day, 1983. A strong jet stream was located along the eastern seaboard at this time, and over the preceding 24 hours noise had been building up in the operational analysis, leading to the picture shown in the upper plot of Fig. 6. The noise subsequently died down, as the jet stream weakened in reality.

The lower plot in Fig. 6 is the result of a 24-hour assimilation incorporating the model changes noted above. A striking reduction in the noise along the jet axis is evident. Elsewhere, the two analyses are notably similar.

Although forecast experiments at the time of the change indicated very little impact on conventional measures of forecast accuracy, isolated cases of detrimental influence of the increased diffusion of divergence were subsequently found. For T106 resolution fields other than divergence are damped at a rate which is larger for the smallest retained scale than was the case for T63, and the coefficient of diffusion of divergence is only $2\frac{1}{2}$ times that of the other fields.

2.4 Modification of the time-stepping in the parametrization of vertical diffusion

Detailed evaluation of the results of test integrations at T106 resolution revealed a marked tendency for noise to develop in the model boundary layer in regions of strong low-level flow. Examination of corresponding T63 forecasts showed a rather similar noise, but of weaker amplitude, and of a larger horizontal scale that could on occasions be confused with small synoptic-scale variations. Apparently similar problems with derivatives of the ECMWF model have been reported by Larsson (personal communications) using a single column version and by Källberg and Gollvik using a limited-area model based on the Centre's original grid-point model. The noise was ascribed to a time-stepping problem in the case of strong vertical diffusion, and a solution was found by utilizing shorter timesteps for this parametrization. This has the disadvantage of increased computational cost.

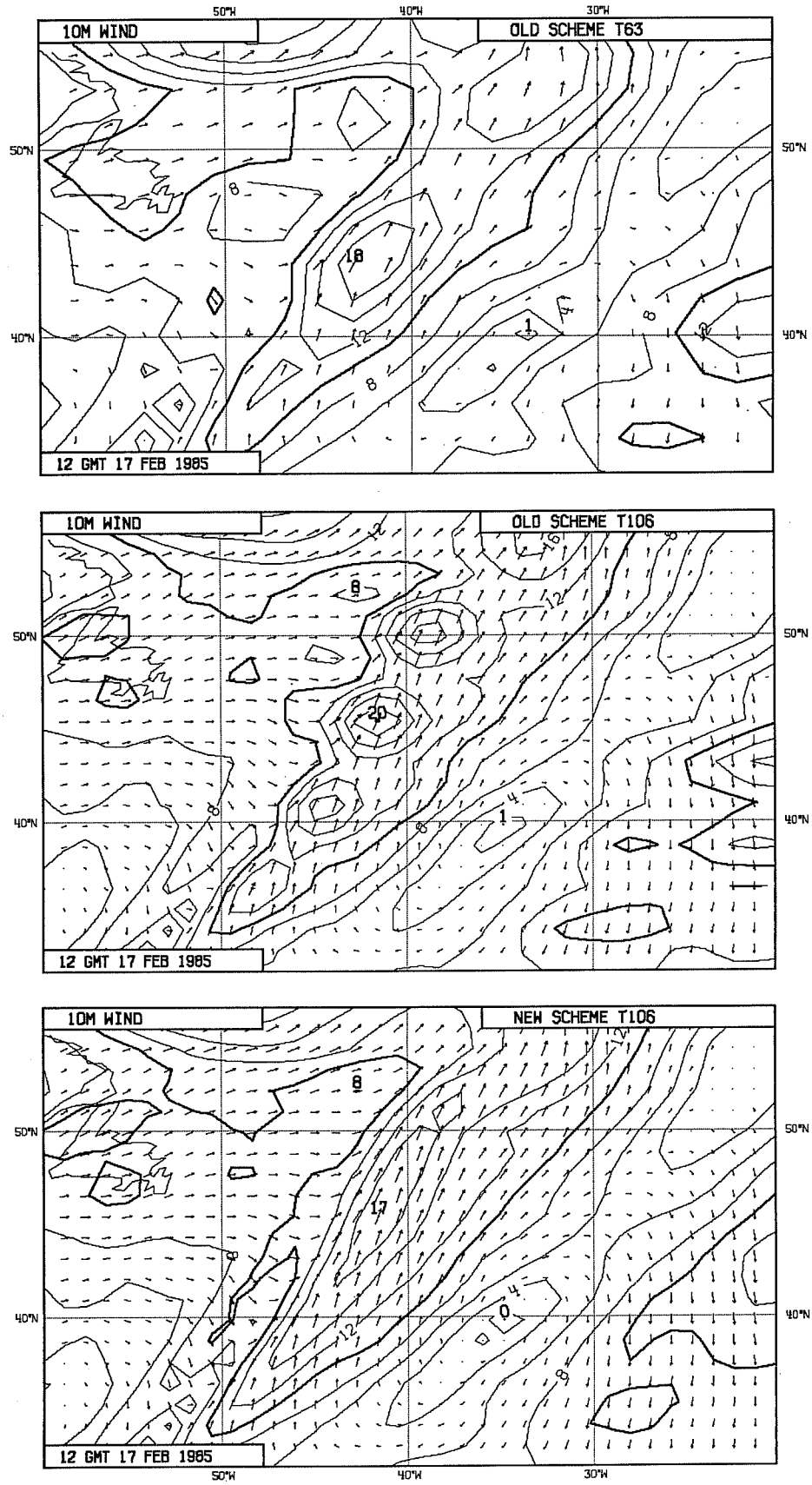

Fig. 7 D+2 forecasts of 10 m wind over the North Atlantic using the former operational time scheme for vertical diffusion at resolution T63 (upper) and T106 (middle). The corresponding T106 forecast with the modified time scheme is shown in the lower map. The contour interval is 2 m s^{-1}.

An efficient remedy to the problem has been found by modifying the time-scheme used to solve the vertical diffusion equation. Writing this equation in the general form

$$\frac{\partial \Psi}{\partial t} = \frac{1}{\rho} \frac{\partial}{\partial z} (\rho \, K(\psi) \, \frac{\partial \psi}{\partial z}) \ ,$$

the tendency due to vertical diffusion was formerly computed in the model as $(\psi^*(t+\Delta t) - \psi(t-\Delta t)) \ / \ 2\Delta t$, where

$$\frac{\psi^*(t+\Delta t)-\psi(t-\Delta t)}{2\Delta t} = \frac{1}{\rho} \frac{\partial}{\partial z}(\rho \, K(\psi(t-\Delta t)) \, \frac{\partial}{\partial z}\psi^*(t+\Delta t)).$$

The solution comprised replacing the $\psi^*(t+\Delta t)$ on the right-hand side of this equation by $1.5\psi^*(t+\Delta t) - .5\psi(t-\Delta t)$. It was suggested by examining the simpler equation

$$\frac{\partial x}{\partial t} = - k|x|x + f$$

for constant k and f. Evaluating $|x|x$ as $|x(t-\Delta t)|x(t+\Delta t)$ yields a solution which oscillates about $\sqrt{\frac{h}{k}}$ with a period $4\Delta t$ in the limit as $\sqrt{(fk)} \ \Delta t \to \infty$. With $x(t+\Delta t)$ replaced by $\gamma x(t+\Delta t) + (1-\gamma)x(t-\Delta t)$, the oscillation is damped by a factor $\frac{2-\gamma}{\gamma}$ each timestep for $\gamma > 1$. Tests in the full model with $\gamma = 1.25$, 1.5 and 2 showed the first value to be insufficient to control fully the noise. Very similar results were obtained with the other two values, the smaller one being chosen as it gives a smaller truncation error for weak diffusion coefficients.

An example of the impact of the change on one of the disseminated ECMWF products, the wind extrapolated to a 10 m height from the lowest level of the model, is shown in Fig. 7. Illustrated are three two day forecasts for a case of strong southwesterly flow over the central North Atlantic Ocean. The T106 forecast with the former time-stepping for the vertical diffusion equation clearly exhibits a sequence of maxima and minima in wind strength, and some indication of this is perhaps also evident in the corresponding T63 forecast. The revised scheme clearly gives a much more uniform low-level flow, and

vertical structure in the boundary layer is similarly improved. It was introduced operationally at the same times as the T106 resolution.

3. HORIZONTAL RESOLUTION STUDIES

3.1 Comparisons of T63 and T106

Two series of experiments have been carried out to provide an extensive comparison between spectral-model forecasts with different horizontal resolutions. The first comprises a group of 24 cases spanning the two years prior to the operational introduction of T106 resolution in May 1985. Forecasts were produced with T21, T42, T63 and T106 resolutions. The second consists of T63 and T106 forecasts for 48 cases covering the two years since May 1985. In this section we summarize results, principally in terms of objective verification. Synoptic examples of sensitivity to horizontal resolution are presented in Sections 3.2 and 3.3

Initial analyses for the first series were derived from the operational (T63) analyses for the 15th of each month from May 1983 to April 1985. Experiments were carried out using two different prescriptions of the orography for each resolution (and a third for T106). The results of these experiments are described by Jarraud et al. (1988); here we present only one set of results produced using an "envelope" orography based on adding $\sqrt{2}$ times the standard deviation of the actual subgridscale orography to the grid-square mean (the operational choice for T63).

The second series comprised forecasts run from the 1st and 15th of each month from May 1985 to April 1987. The operational T106 forecasts (with one standard-deviation envelope orography) served as controls, and corresponding T63 forecasts were carried out from truncated T106 analyses, using the same parametrizations and model settings apart from the coefficients of horizontal diffusion. For the latter, the previously operational T63 values were used for the first 15 cases, after which the coefficient for divergence was reduced from 20 to 5 x 10^{15} m^4 s^{-1}, 2.5 times larger than that for other fields. All T106 forecasts used diffusion coefficients half those used latterly for T63.

Anomaly correlations of 500 mb height for the extratropical Northern Hemisphere, averaged over the two sets of cases, are presented in Fig. 8. The upper plot shows, not surprisingly, a much larger improvement of T42 over T21

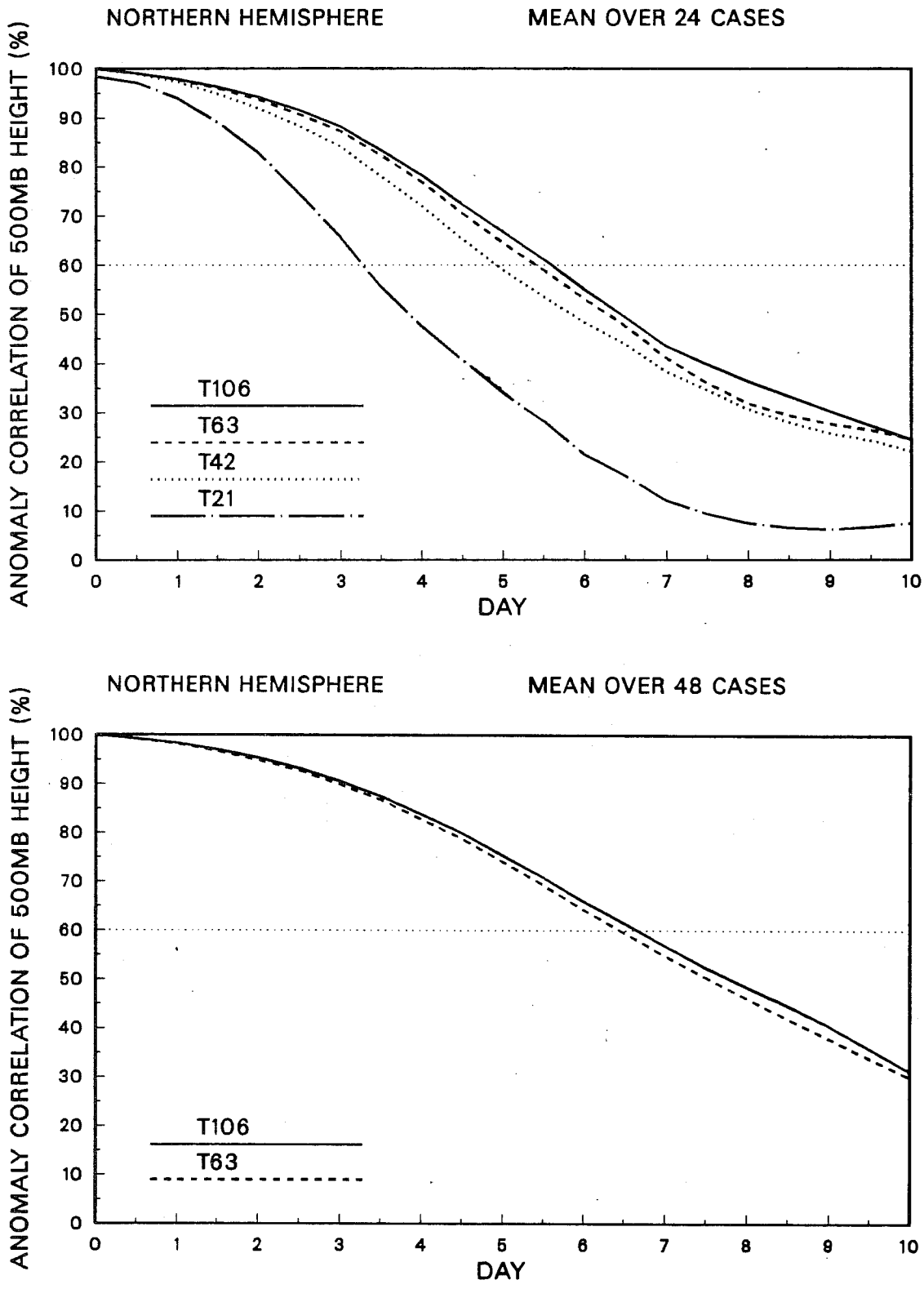

Fig. 8 Anomaly correlations of 500 mb height for the extratropical Northern Hemisphere averaged over sets of 24 (upper) and 48 (lower) cases, for spectral truncations T21, T42, T63 and T106 as indicated in each panel.

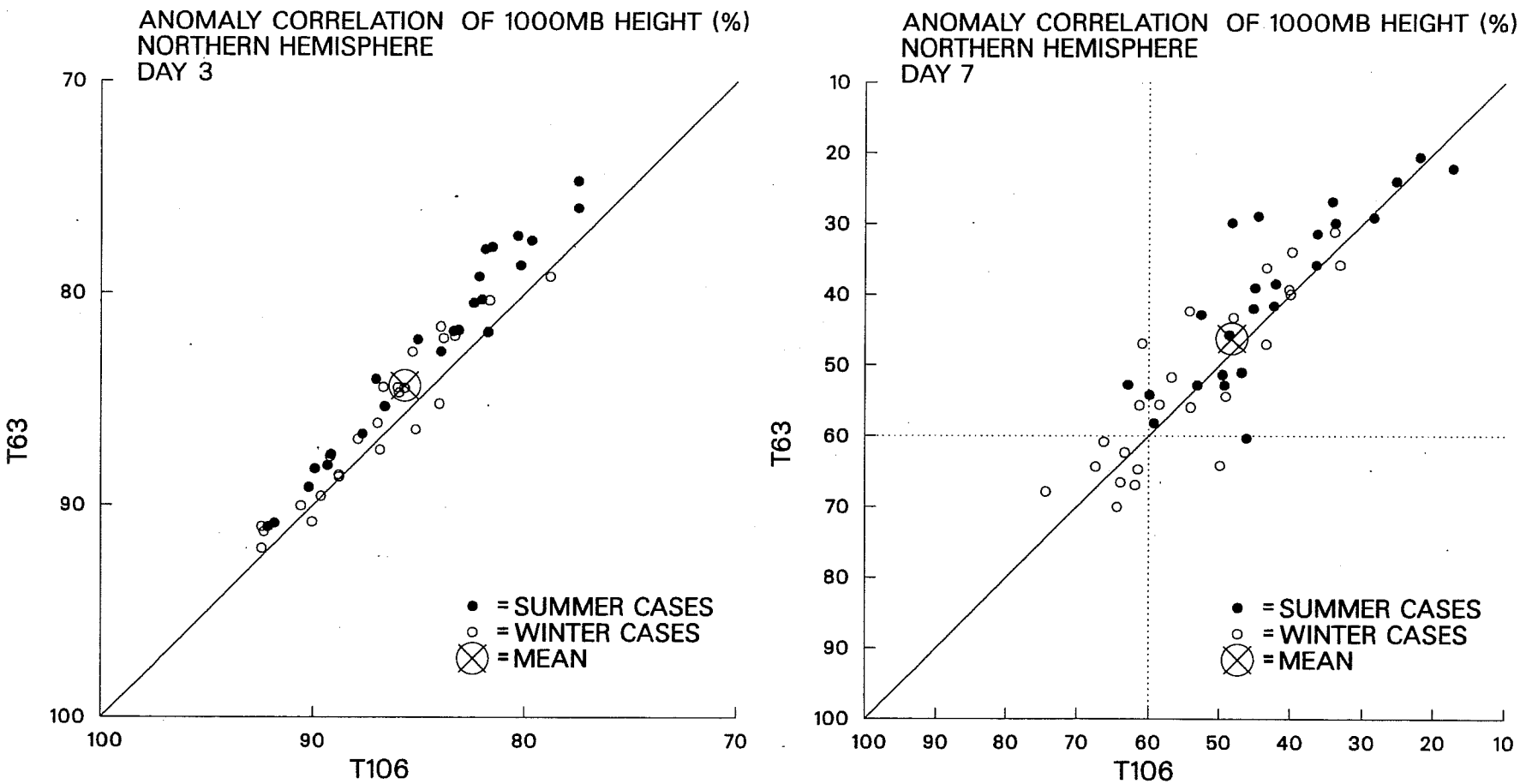

Fig. 9 Scatter diagrams of anomaly correlations of 500 mb height for the extratropical Northern Hemisphere, comparing T63 and T106 forecasts at day 3 (left) and day 7 (right). Points lying above the diagonal indicate better performance of T106. Solid circles denote summer cases, open circles denote winter cases, and crosses denote the means.

than that of T63 over T42, which in turn is larger than the improvement of T106 over T63. This tendency for convergence at high resolution does not, however, imply that differences between T63 and T106 are small throughout the forecast range, but rather that what can be quite large differences later in the forecast range are not systematically in clear favour of the higher resolution, as will be seen shortly. The apparently small mean differences in skill are nevertheless larger than differences found earlier between the Centre's N48 grid-point and T63 spectral forecasts, and larger than differences between forecasts using mean and envelope orographies. Other objective measures of forecast skill for the Northern Hemisphere generally confirm the picture shown in Fig. 8, although standard deviations exhibit more favourable results for T42, and to some extent T63, towards the end of the forecast range, a finding which is presumably related to the higher level of variance that is found in the higher resolution forecasts.

Comparing the two panels in Fig. 8, it can be seen that differences between T63 and T106 are very much the same in the two sets of experiments, despite differences in the parametrizations, envelope orography, and resolution of the assimilating model (T63 or T106) used to produce the initial analyses. Later in the forecast range a more uniform difference between T63 and T106 is seen in the second, larger set of cases. Perhaps more noteworthy is the large overall difference in forecast quality between the two sets of cases, both T63 and T106 forecasts crossing the line denoting 60% correlation about 1 day later in the second set than in the first. Although interannual variability in the inherent predictability of the atmosphere may contribute to this difference, it is likely that it largely reflects advances in data assimilation (including the use of a higher resolution model) and parametrization, and perhaps the improved stratospheric resolution of the forecast model.

Early in the forecast range differences between T63 and T106 for individual cases are almost systematically in favour of the higher resolution. This is seen particularly clearly at the surface, and is illustrated in the left-hand part of Fig. 9, which plots (from the second set of experiments) each case on a scatter diagram for the anomaly correlation of 1000 mb height for 3-day forecasts for the extratropical Northern Hemisphere. Points lying above the diagonal line correspond to cases in which T106 is (according to the measure

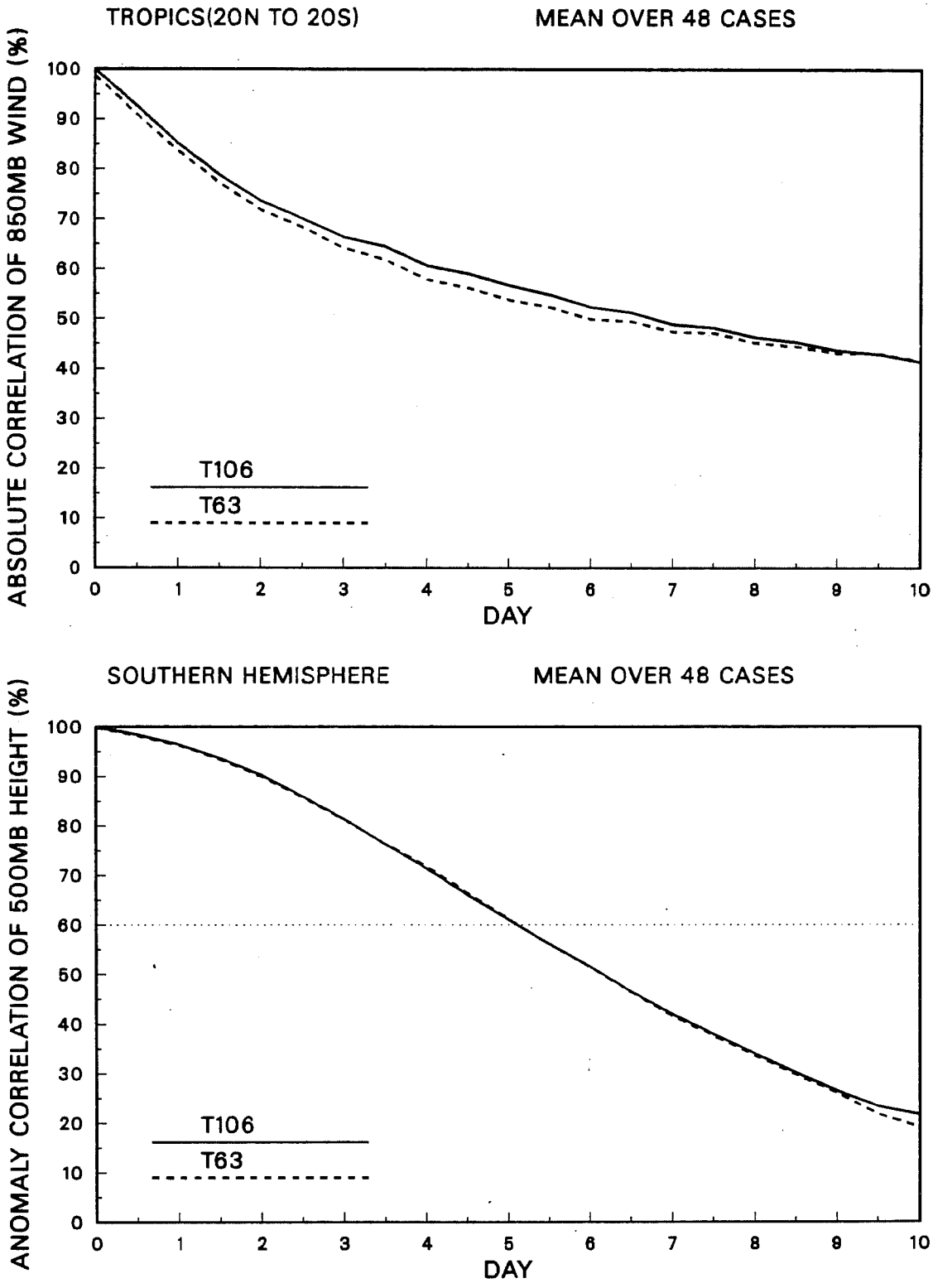

Fig. 10 Absolute correlations of 850 mb vector wind for the Tropics (upper) and anomaly correlations of 500 mb height for the extratropical Southern Hemisphere (lower), averaged over 48 cases for T106 (solid) and T63 (dashed) forecasts.

in question) better than T63, and it can be seen that at day 3 by far the majority of points lie above the line. The plotted points distinguish between "summer" (May to October) and "winter" (November to April) cases, and the advantage of T106 over T63 at day 3 is particularly evident in summer, only one out of 24 cases failing to show an improvement. This is related in part to the choice of envelope orography, since it has been found (Jarraud et al., 1988) that the impact of envelope orography is beneficial at both T63 and T106 resolution in winter, whereas in summer the envelope orography gave poorer mean anomaly correlations than did mean orography for T63, with similar correlations for the two orographies for T106.

The corresponding scatter diagram for day 7 is also shown in Fig. 9. At this range there is evidently more spread, and a less systematic bias in favour of T106. A more beneficial impact of higher resolution in summer than in winter cases can again be discerned. It is noteworthy, however, that at both days 3 and 7 there is considerably more spread along the diagonal than across it; differences in forecast accuracy from case to case are generally much larger than differences resulting from the resolution change.

Objective verification has been carried out for a number of regions other than the extratropical Northern Hemisphere. Absolute correlations of 850 mb vector wind for the Tropics and anomaly correlations of 500 mb height for the Southern Hemisphere, averaged over the second set of cases, are presented in Fig. 10. There is a distinct improvement of T106 over T63 in the tropical verification, and a negligible net sensitivity to resolution in the results for the Southern Hemisphere. Similar conclusions were drawn from verification of the first set of cases, although smaller differences are found in the tropical region, with T63 in fact scoring better than T106 out to day 2.5. This may reflect a difference in sensitivity to resolution for the two versions of the convective parametrization used in these experiments, but it could also indicate sensitivity of the short-range forecast to compatibility between the resolution of the forecast model and that of the assimilating model, which was T63 for the first set of experiments and T106 for the second.

The extent to which differences in orography and horizontal diffusion contribute to the differences between T63 and T106 has been examined in a

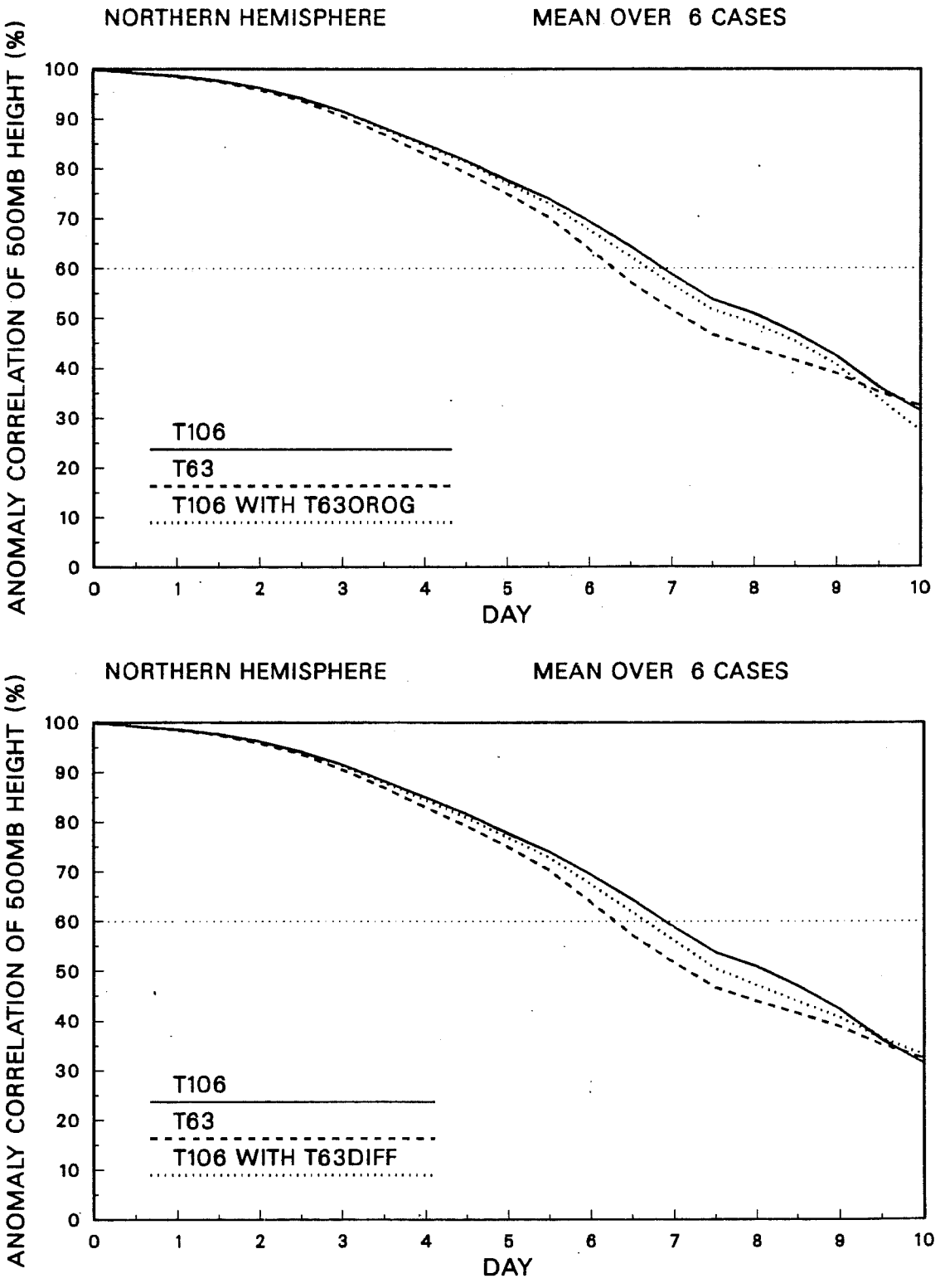

Fig. 11 Mean anomaly correlations of 500 mb height for the extratropical Northern Hemisphere, for 6 cases carried out at T106 (solid) and T63 (dashed) resolution, and for T106 forecasts carried out with T63 orography (dotted, upper panel), and with T63 diffusion coefficients (dotted, lower panel).

subset of six cases particularly sensitive to the change in resolution. The cases were chosen from among the 24 of the second year of the 48-case series, on the basis of one per two months, choosing out of the four available for each period that for which differences between T63 and T106 forecasts were largest. These cases were also used for the time-step experiments reported in Section 2.2. Six T106 forecasts were carried out using a T63 representation of the orography, and second subset used T106 orography, but the diffusion coefficients used for T63. Results are shown in Fig. 11 in terms of anomaly correlations of 500 mb height for the extratropical Northern Hemisphere. Both finer-resolution orography and smaller diffusion coefficients evidently contribute to the improvement of T106 over T63. Perhaps surprisingly, a somewhat larger impact from diffusion than from orography is seen in Fig. 11, but the reverse is found to be the case for anomaly correlations of 1000 mb height and for standard deviations of the height field errors. The small number of cases must also be borne in mind.

Examples of local beneficial impacts of increased horizontal resolution which are almost certainly related to increased resolution of the model orography will be discussed in the following two sections. To counterbalance these, Fig. 12 presents a case (specially selected from the first set of comparisons) where use of higher-resolution orography contributed little to a substantial improvement of T106 over T63 in the second half of the forecast range. Illustrated are mean 500 mb heights for days 5 to 10 for standard T106 and T63 forecasts, for a T106 forecast with T63 orography, and for the verifying analysis. The standard T106 forecasts accurately matches the analysis in its depiction of the blocking pattern centred over Northern Europe, in contrast to the performance of T63, which produces a block, but with a quite erroneous flow pattern. Running the T106 forecast with T63 orography reproduces much of the detail of the standard T106 forecast, although some deterioration in the trough extending southeastwards from southern Greenland can be seen. This predominant insensitivity to orographic resolution occurs in this case despite a marked sensitivity to the use of envelope orography, as indicated by Jarraud et al. (1988).

Sensitivity to the magnitude of horizontal diffusion has been examined in cases other than those contributing to the mean results shown in Fig. 11. Although these generally confirm the choice made at the time of operational

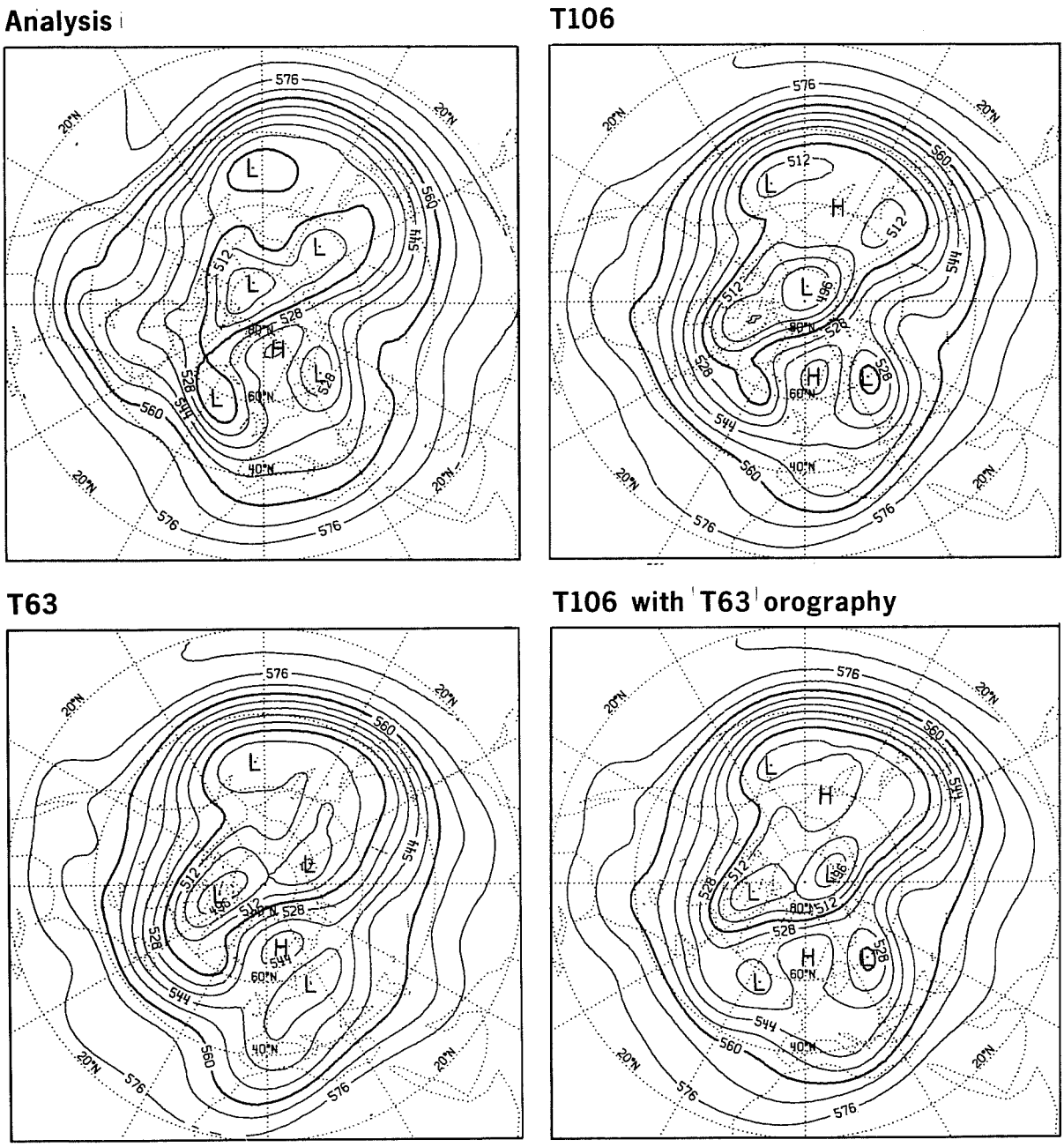

Fig. 12 Mean analyzed 500 mb height field (contour interval 8 dam) for the period 20-25 March 1984 (upper left), and corresponding forecasts from 15 March using:
Upper right - T106 resolution (and orography)
Lower left - T63 resolution (and orography)
Lower right - T106 resolution but T63 orography.

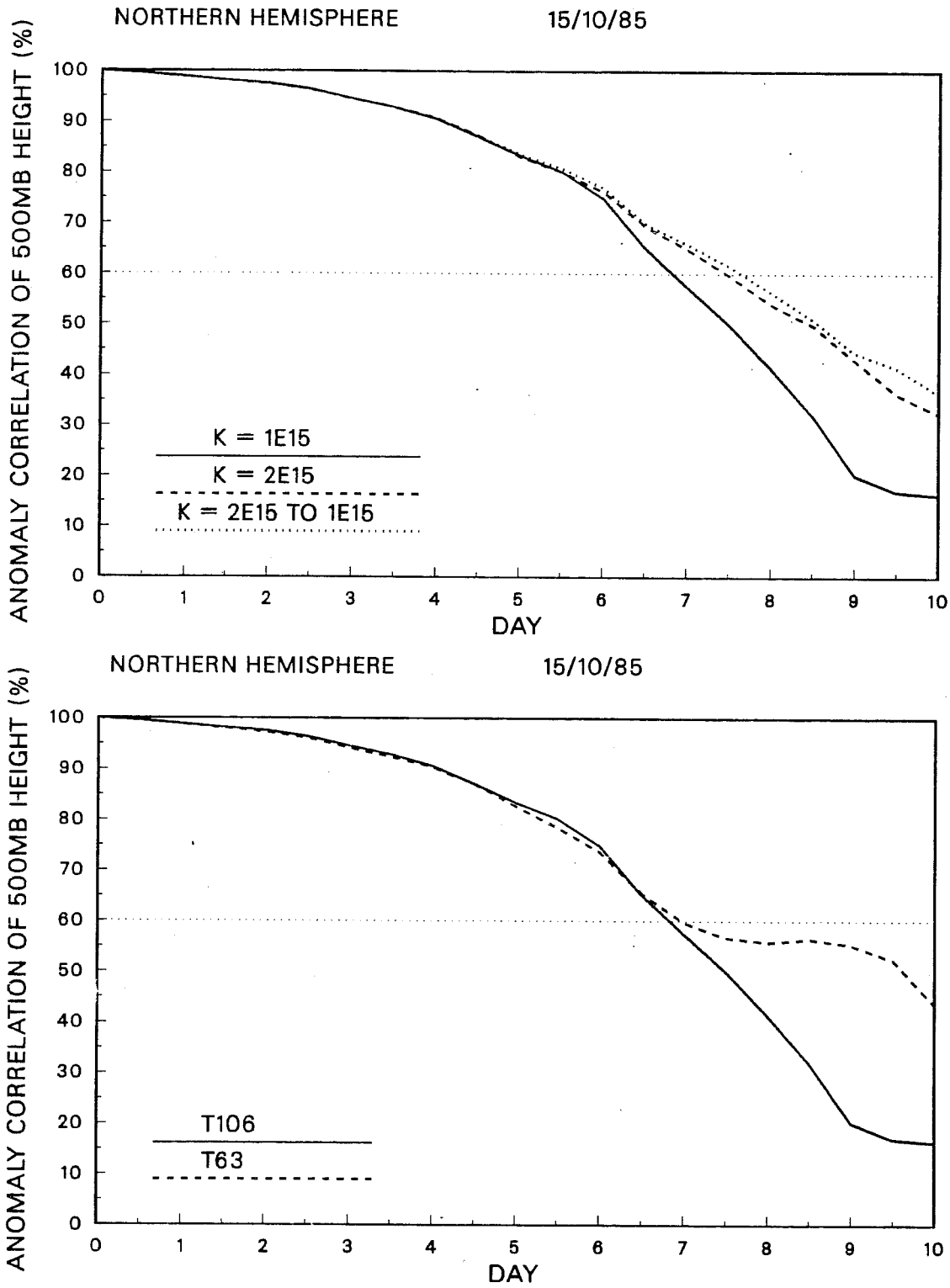

Fig. 13 Anomaly correlations of 500 mb height for the extratropical Northern Hemisphere, for forecasts from 15 October 1985. The upper panel shows T106 results obtained with standard horizontal diffusion coefficients (solid line), with coefficients twice the standard value (dashed), and with coefficients which reduce from the larger to the smaller values between days 1 and 2 (dotted). T106 and T63 forecasts are compared in the lower panel.

implementation of T106 resolution, clear exceptions are found. A striking example is presented in Fig. 13. In this case doubling the coefficients of horizontal diffusion had a clear benefit for the T106 forecast beyond day 6, as seen from the objective verification in the upper panel of the figure. The corresponding T63 forecast also showed a much less rapid fall in skill than did the standard T106 at the end of the forecast range (lower panel). It was observed in this case that there was a much more pronounced than usual "spin-up" of vertical velocity in the tropics. The T106 forecast was thus rerun with the higher level of diffusion for the first day only, reducing it linearly to the standard lower value between day 1 and day 2. Objective verification for the extratropical Northern Hemisphere, shown also in the upper panel of Fig. 13, indicates a performance very similar to (and slightly better than) that of the forecast which used higher diffusion throughout the 10-day range. Synoptic assessment confirms both this result, and that a substantial part of the improvement of T63 over T106 beyond day 7 has the same synoptic character as the improvement of T106 forecasts by use of higher horizontal diffusion.

3.2 First results from T159

A limited programme of experimentation was begun in 1986 with the spectral model at a resolution of T159. This resolution was chosen because it was the largest that could be run with acceptable efficiency within the memory constraints of the Centre's computer system, although each forecast took too long a time to be operationally feasible (8-9 hours for the 16-level vertical resolution used for the first experiments). A one standard deviation envelope orography with T159 resolution was used, and initial and other surface fields were interpolated from operational T106 fields. The operational T106 forecasts were available for comparison, and T42 and T63 forecasts were also carried out. Three 10-day predictions were initially run, and these were subsequently supplemented by three one-day forecasts for cases of rapid oceanic cyclone development.

An initial date of 20 March 1986 was chosen for the first case because of an Alpine lee cyclogenesis early in the forecast range which was underestimated by the operational forecast. Clear improvements were found with increasing resolution, both in the intensity and position of the cyclone, and in the detail of local flow patterns near orography (Simmons et al., 1988). These

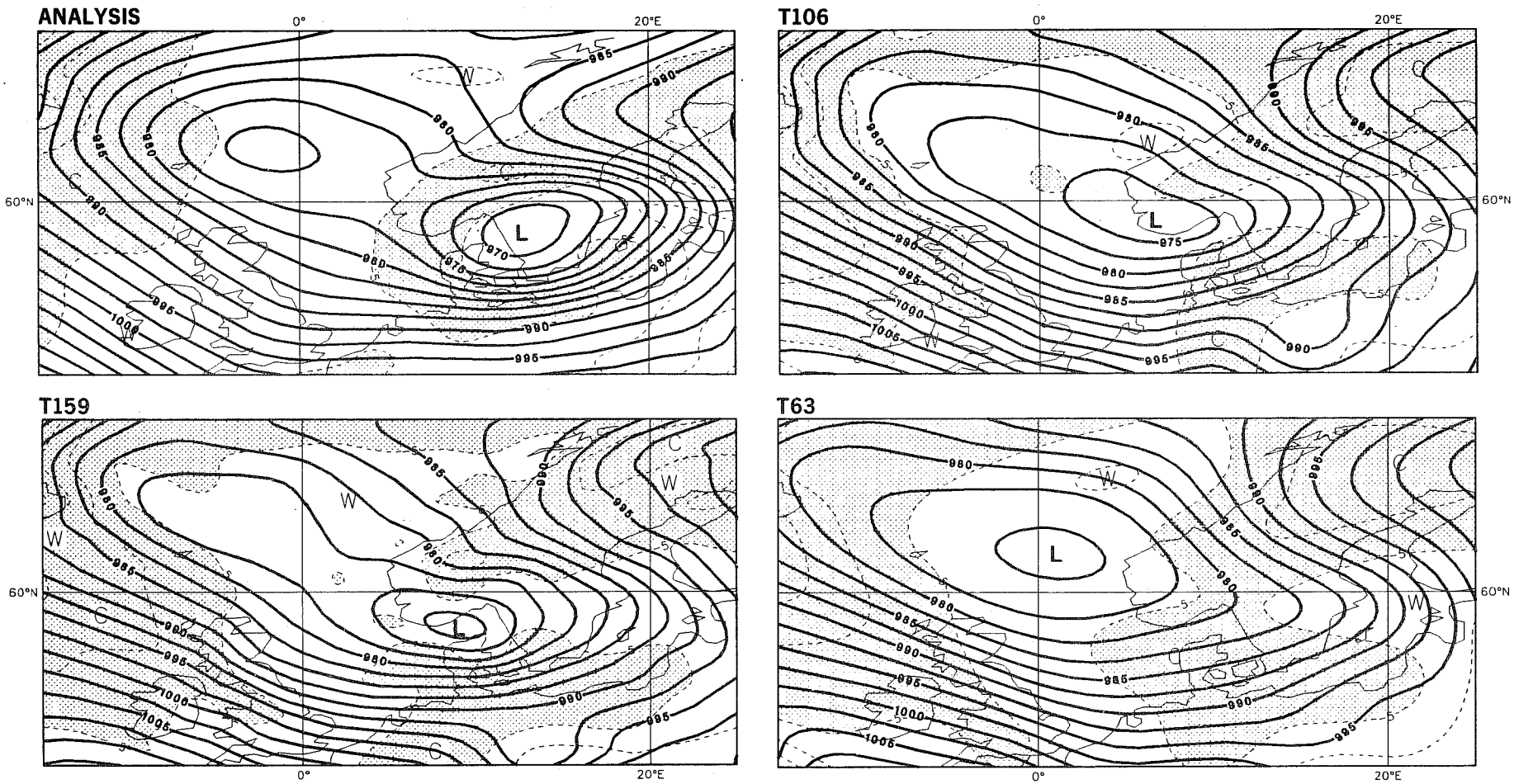

Fig. 14 The operational (T106) analysis for 12Z, 25 March 1986 (upper left), and 5-day forecasts valid at this time performed using horizontal resolutions T106 (upper right), T159 (lower left) and T63 (lower right). Solid lines show mean sea-level pressure with a contour interval of 2.5 mb, and 850 mb temperature is denoted by dashed contours, with 2 K interval, and by shading values below -5°C.

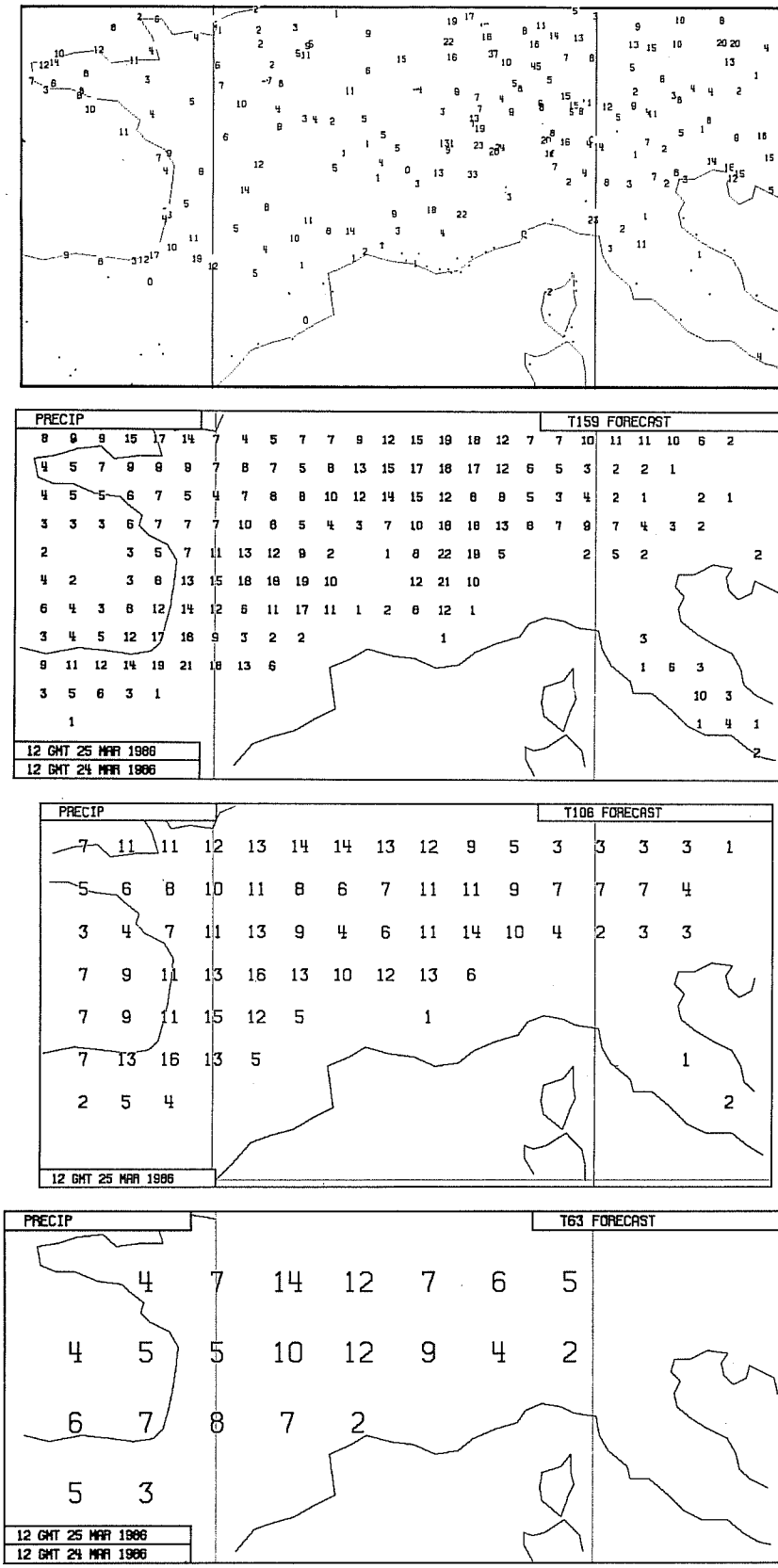

Fig. 15 24-hour net precipitation (mm) for the period 12Z, 24 March to 12Z, 25 March 1986. Observed values are shown in the upper plot, and predicted values are for T159 (upper middle), T106 (lower middle) and T63 forecasts from 20 March 1986.

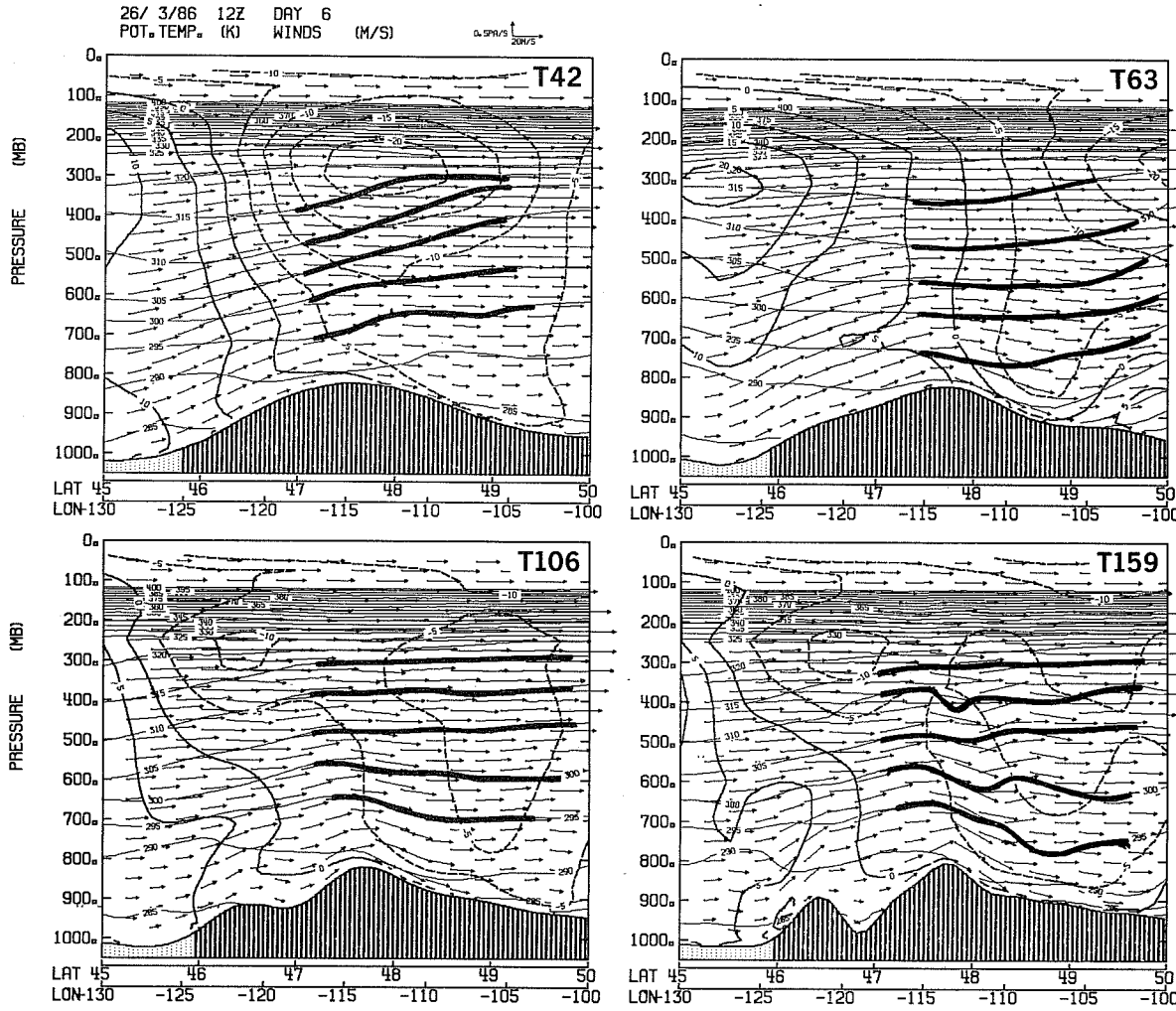

Fig. 16 Cross-sections of potential temperature and winds from 45°N, 130°W to 50°N, 100°W for day 6 forecasts from 20 March 1986, using resolutions T42 (upper left), T63 (upper right), T106 (lower left) and T159 (lower right).

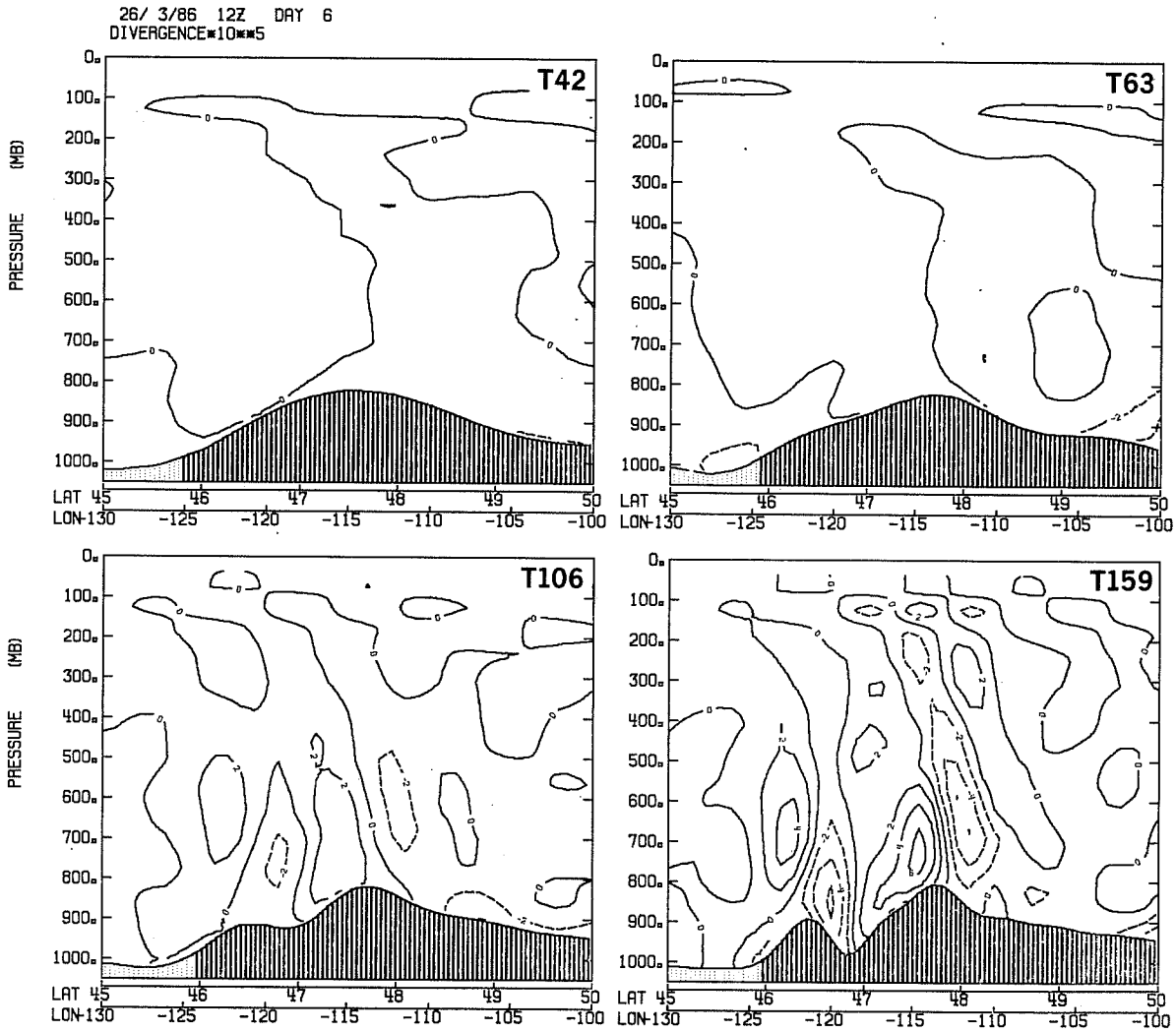

Fig. 17 Cross-sections of divergence from 45°N, 130°W to 50°N, 100°W for day 6 forecasts from 20 March 1986, using resolutions T42 (upper left), T63 (upper right), T106 (lower left) and T159 (lower right).

are not illustrated here as a second example of lee cyclogenesis will be discussed in the following section. Instead, we present a variety of other results from this case.

In the middle of the forecast range, synoptic differences became apparent over northern Europe. Fig. 14 illustrates how the 5-day prediction of a low which was located in reality over southern Sweden is progressively and significantly improved as resolution is increased. T159 also gives the best indication of a second, weaker low to the west. There is much less synoptic difference between T63, T106 and T159 over southern Europe (not shown) at this time, but quite distinct sensitivity in the prediction of precipitation can be seen in Fig. 15. In most respects the expected increase in detail with increasing resolution is such as to bring forecast and observation closer together.

As horizontal resolution increases, models can be expected to represent a larger degree of explicit orographically-induced gravity wave activity. Fig. 16 presents cross-sections of wind and potential temperature at day 6 of the T42, T63, T106 and T159 forecasts, again for the 20 March initial conditions. Each section cuts through the Cascade and Rocky Mountain chains of western North America, although only T106 and to a greater extent T159 resolutions are capable of distinguishing between the two ranges. Over this area, the large-scale forecasts are rather insensitive to horizontal resolution, with a predominantly westerly incident flow. Small-scale wave motion over and immediately downstream of the Rockies ridge is evident in the T159 forecast, but not at lower resolutions.

The forecasts discussed above were carried out without the parametrization of gravity-wave drag. There is an evident possibility (ECMWF, 1987) that as resolution increases, effects of gravity waves which in reality occur on scales close to the truncation limit may appear twice in the model, once through parametrization and once explicitly. Quite apart from this problem, the explicit appearance of vertically-propagating gravity waves brings the question of the upper boundary condition to the fore. Cross-sections as in Fig. 16, but for the divergence field, are presented in Fig. 17 and show a westward phase tilt with increasing height in the troposphere over the Rockies at T159 and T106 resolutions. However, there is an absence of tilt in the

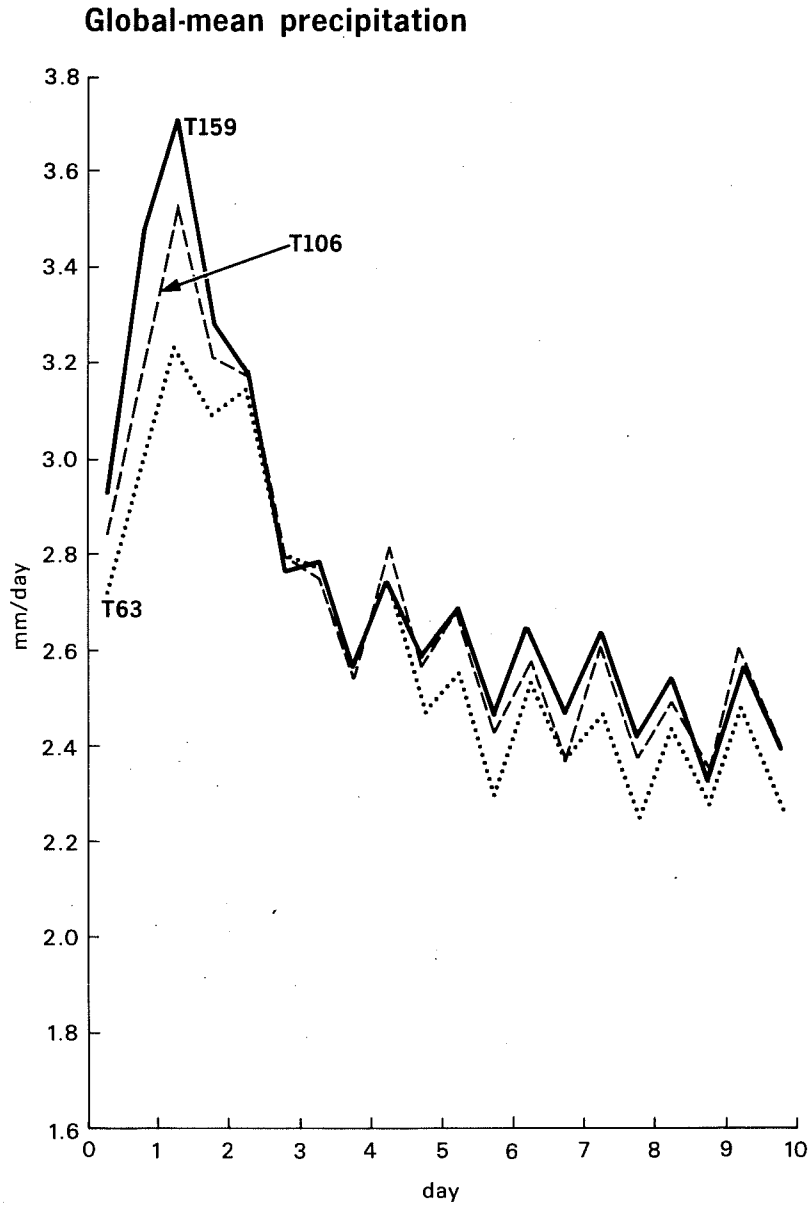

Fig. 18 Global-mean precipitation rates for T159 (solid), T106 (dashed) and T63 (dotted) forecasts from 20 March 1986.

stratosphere which is suggestive of an erroneous wave reflection due to the inadequate treatment of upward propagating waves in the topmost layers of the model. These forecasts were all carried out using the formerly-operational 16-level resolution. During testing of the increased stratospheric resolution of the now-operational 19-level version, more extreme cases where strong mountain waves appeared explicitly at T106 and T63 truncations were examined. These showed a more severe stratospheric problem at higher vertical resolution, with the occurrence at small horizontal scales of pronounced two-grid waves in the vertical at upper model levels. This led to the use of higher horizontal diffusion in the stratosphere of the operational 19-level model, an apparently effective remedy, at least for the short term, but one which should not be seen as obviating the need for a much more thorough study of this topic as horizontal and vertical resolution increase further.

The use of increased horizontal resolution, with its attendant reduction in horizontal diffusion coefficients, is generally found to exacerbate the problem of the "spin-up" of excessive vertical velocities and convective precipitation in the tropics early in the forecast range. This is illustrated in Fig. 18 by plots of global-mean precipitation rates as functions of forecast range, for T63, T106 and T159 forecasts from 20 March 1986. There is a significant increase, as resolution increases, in the unrealistically high rates found in the first $2\frac{1}{2}$ days, and a smaller increase beyond this time. Examining the breakdown into convective and large-scale precipitation reveals a predominant increase in the convective component in the early part of the forecast range, the smaller increase later on being associated with more large-scale rather than convective precipitation.

One further pre-existing modelling problem has been found to become more pronounced in the T159 forecasts. The early experimentation with T106 revealed a tendency for "noise" to develop in the planetary boundary layer in cases of strong flow over ocean surfaces, which was remedied by revising the time-stepping algorithm used in the parametrization of vertical diffusion, as discussed in section 2.4. This solution has worked satisfactorily at T106 resolution, but occasional instances of a return of "noise" at T159 resolution have been found. Fig. 19 illustrates roughness in temperature contours along a warm front, and the presence of small-scale low-level ascent and descent in the flow along the front. Although the corresponding T106 forecast was

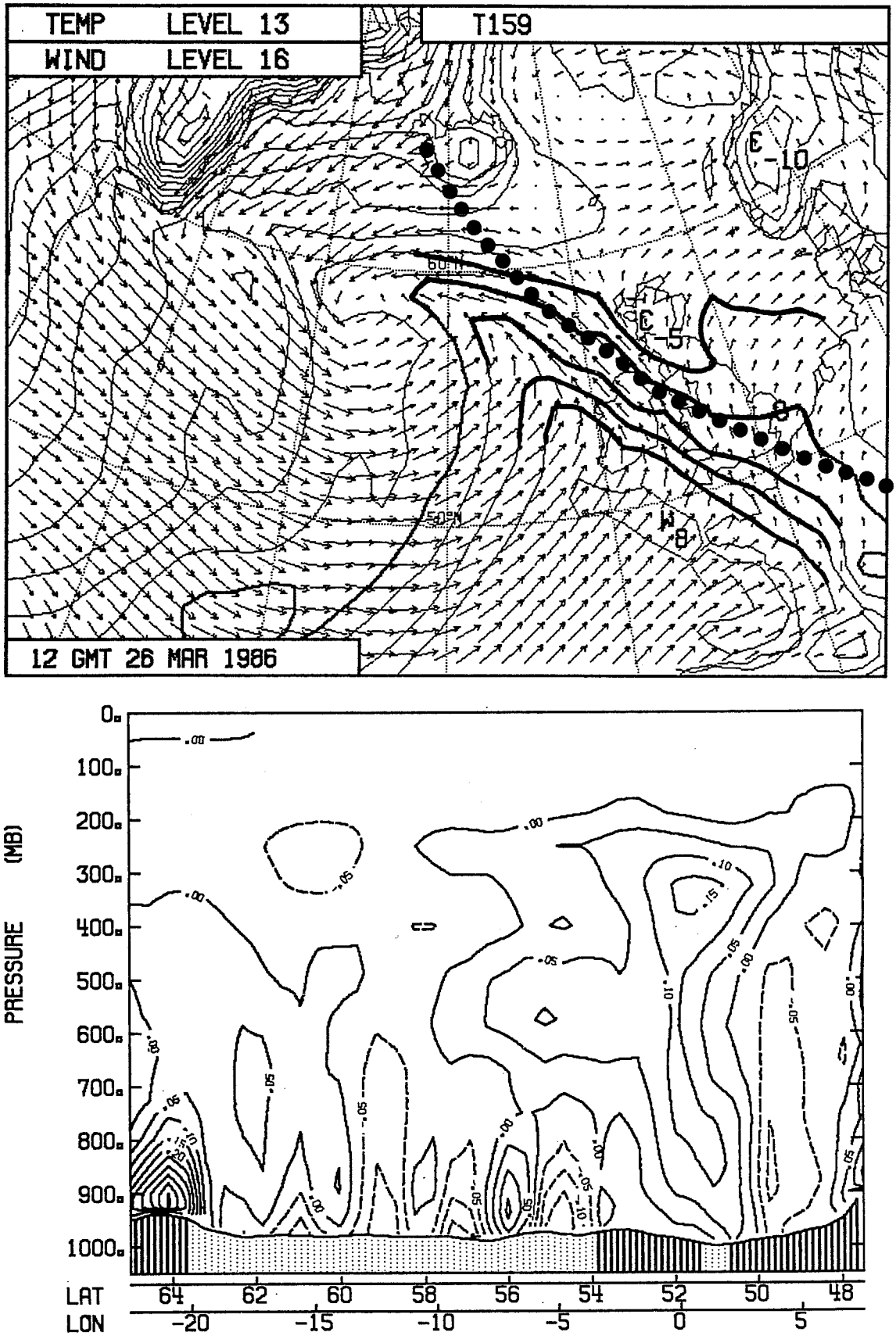

Fig. 19 Upper panel: Wind at the lowest model level (level 16) and temperature (contour interval 2 K) at level 13 for the 6-day T159 forecast from 20 March 1986.
Lower panel: The corresponding cross-section of vertical velocity (Pa s^{-1}) taken along the dashed line shown in the upper panel.

somewhat poorer in synoptic detail, it did not exhibit these presumably spurious small-scale features.

It is important, however, to stress that the problem illustrated above is very much an occasional one, and notwithstanding the need for improving the computational stability of the boundary-layer calculation, sharper and more coherent frontal structures are generally found in the T159 forecasts. One of the cases of rapid cyclone growth is shown in Fig. 20. Strong development is found at all three horizontal resolutions (the central pressure was 989 mb 24 hours earlier), but the depth of the low is captured most accurately with T159. It is more difficult to verify differences in thermodynamic structure between T159 and T106 because of the bias of the verifying analysis towards the T106 resolution used in the data assimilation, but the waviness of the cold front at T63 resolution disagrees with the analysis, with the higher resolution forecasts and with satellite imagery. Some of this waviness can also be seen in the T106 forecast, and the occlusion is less advanced and well-defined (and more inaccurate) at this resolution than at T159. Similar results have been found in other cases.

3.3 Further studies of increased horizontal resolution

A further five cases have been chosen for study of increased horizontal resolution. Four were selected on the basis of an interesting weather development in the short range, to enable global forecasts to be compared with forecasts at resolutions higher than T159 carried out with the spectral limited-area model being developed at ECMWF. Three of these have been integrated to 10 days using the global spectral model at T63, T106 and T159 resolution. The fourth was integrated only to day 3, a fifth case being chosen for 10-day forecasting as it was realized that the sample would otherwise not have included a high-summer case. The set of global forecasts has only recently been completed, and here we present first impressions of the results on a case-by-case basis.

(i) 3 March 1982

This initial date was chosen from within the ALPEX period because of the occurrence over the following two days of a lee cyclogenesis which has been much studied subsequently. In particular, sensitivity to horizontal

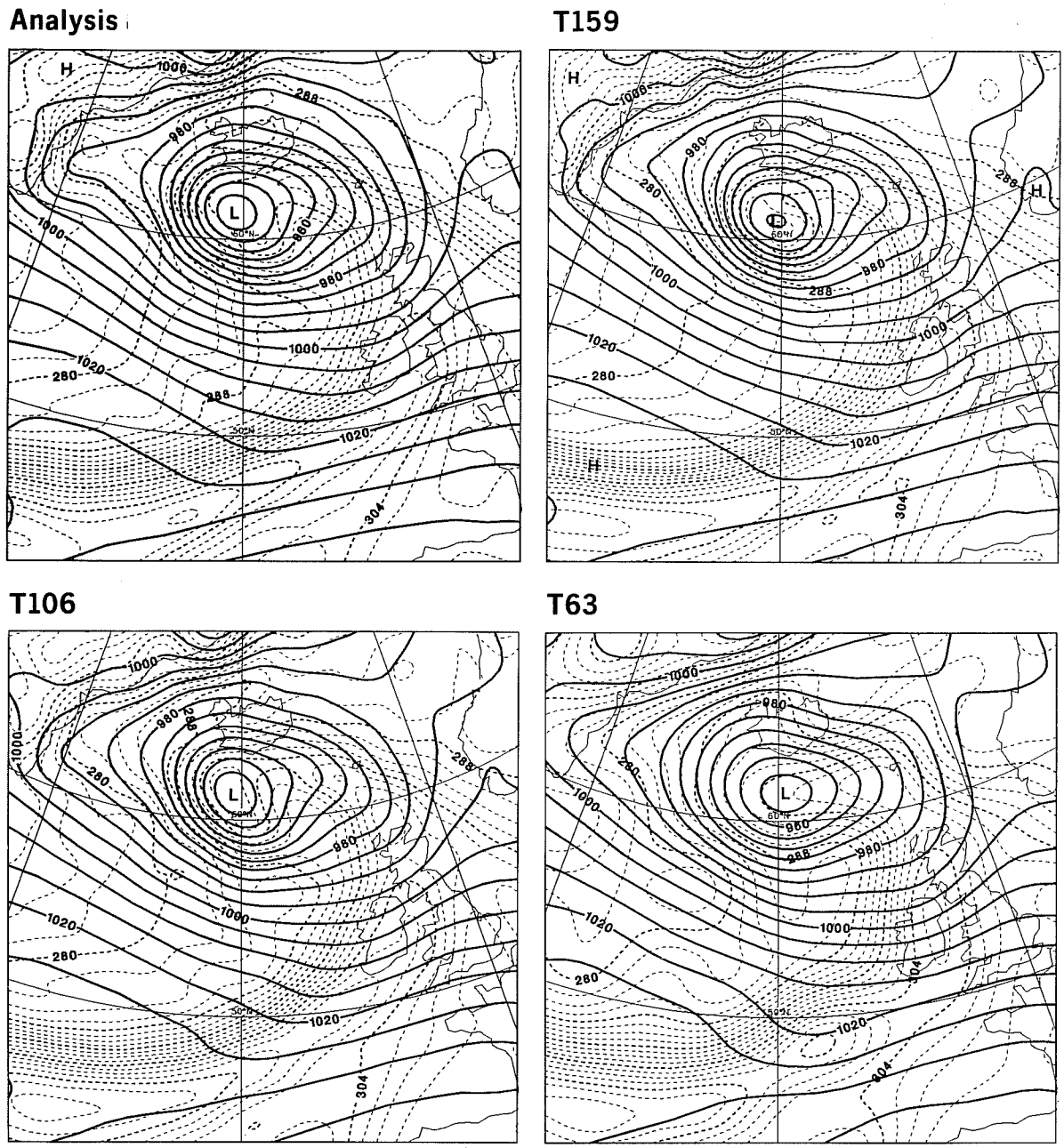

Fig. 20 The operational analysis of mean sea-level pressure and 850 mb equivalent potential temperature for 13 January 1986 (upper left), and one-day T159 (upper right), T106 (lower left) and T63 (lower right) forecasts verifying on this date. Contour intervals are 5 mb and 2 K respectively.

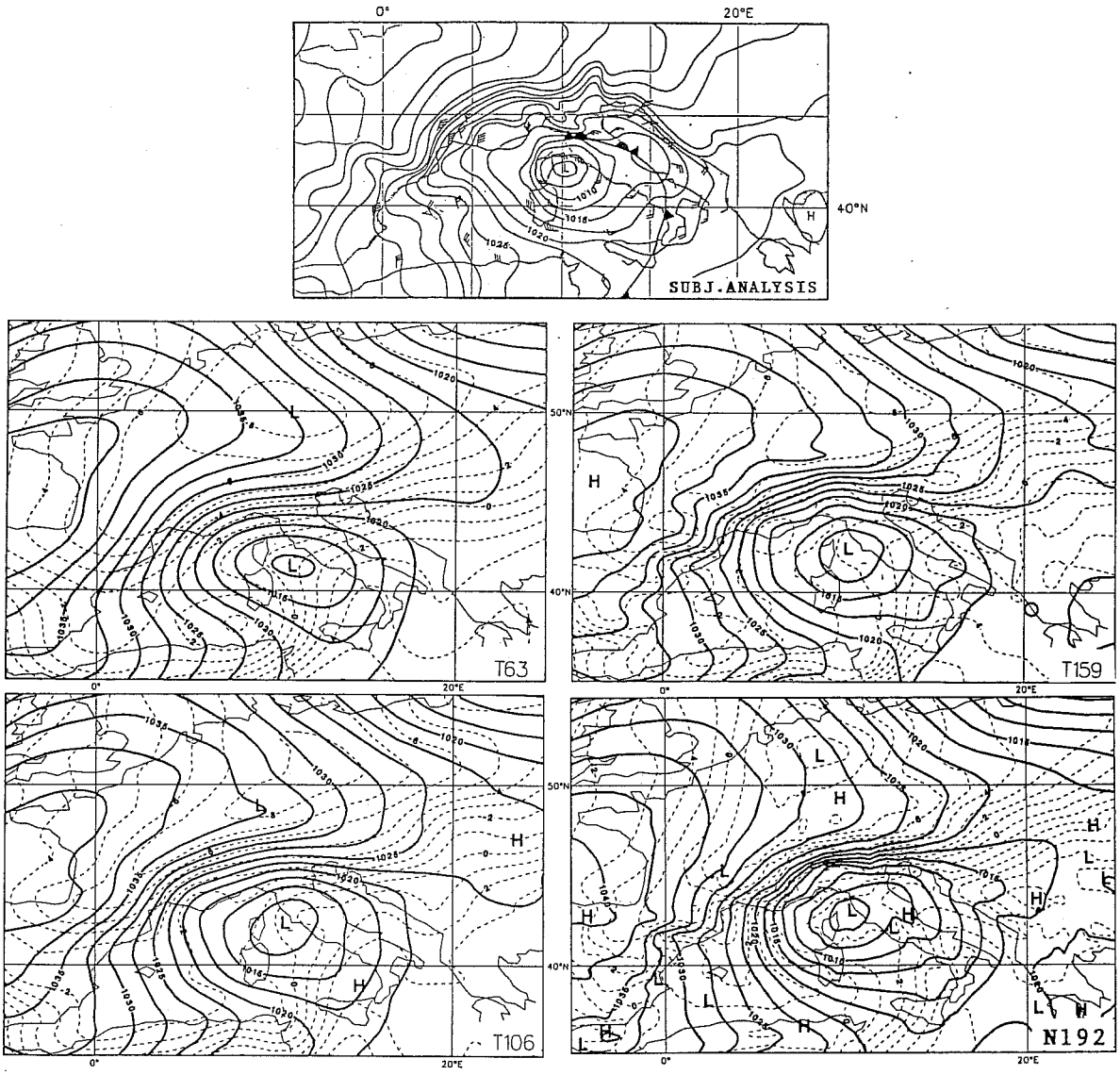

Fig. 21 A subjective analysis of mean sea-level pressure (contour interval 2.5 mb) for 5 March 1982 (upper), and 48-hour forecasts of mean sea-level pressure and 850 mb temperature (contour interval 1 K) using:
Middle left : Spectral model at T63 resolution
Lower left : Spectral model at T106 resolution
Middle right : Spectral model at T159 resolution
Lower right : Grid-point limited-area model at N192 resolution.

resolution and the use of envelope orography has been examined by Dell'Osso (1984) using the ECMWF grid-point LAM. A period of data assimilation using the current T106 L19 operational system was carried out to provide initial conditions. In Fig. 21 we present a subjective analysis of mean sea-level pressure for 12Z 5 March 1982, and corresponding 48-hour spectral forecasts using T63, T106 and T159 resolutions. The 48-hour grid-point forecast with the finest (.46875°) resolution utilized by Dell'Osso is also shown.

It is clear from Fig. 21 that the change in resolution from T106 to T159 is such as to allow the forecast to capture local detail present in both the analysis and the high-resolution LAM. Particular examples are the pressure patterns near the Pyrenees and the Italian peninsula. In this case there is little change in intensity with increasing resolution in the spectral forecasts, and only a minor refinement of position. A more substantial impact in these respects, and similar improvement in local detail, is found in the 20 March 1986 case discussed earlier. For this ALPEX case the LAM forecast is better with regard to the intensity of the lee cyclone and the apparent barrier presented to the cold front by the Alpine ridge; as this model used a different initial analysis and earlier version of the parametrizations the differences in performance may not be wholly due to differences in horizontal resolution and numerical technique.

(ii) 26 February 1984

This case was chosen because of the availability of detailed observations of a polar low, reported by Shapiro et al. (1987). It was recognized that none of the global resolutions to be used would be sufficiently fine to capture the detailed structure of the low, but it was hoped that the large-scale state would be well enough defined in the initial conditions to make the case a suitable one for studying higher resolution and the performance of different convection schemes using the spectral LAM. Again, a spell of data assimilation using the latest operational system was used to produce initial conditions.

Wind and temperature forecasts at the third model level above the surface are shown for 12Z, 27 February, over the Norwegian Sea in Fig. 22, together with an analysis of aircraft measurements of temperature taken at a rather similar

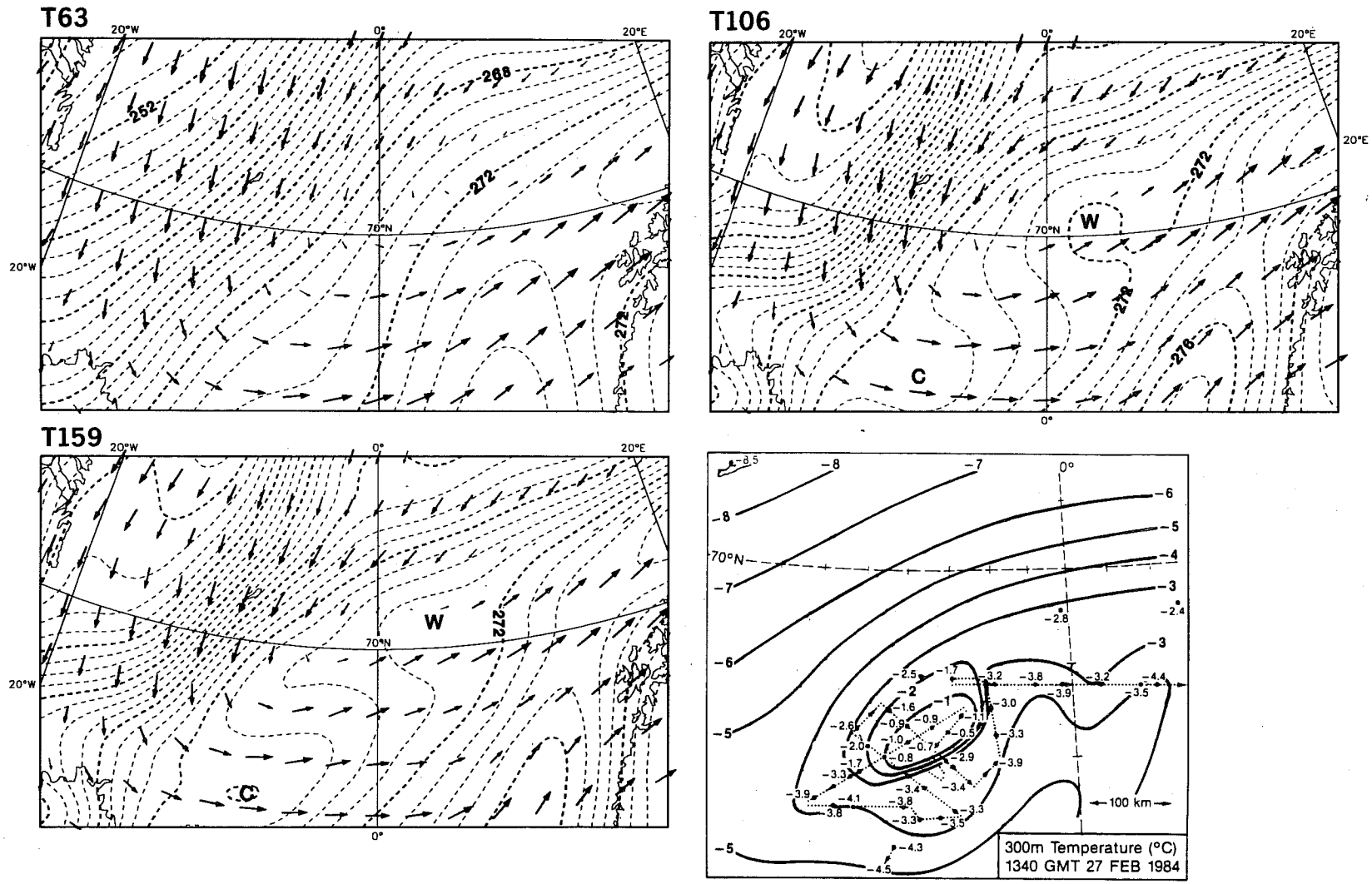

Fig. 22 Wind arrows and temperature contours (interval 1 K) for model level 17 (approximately 370 m) for 1-day T63 (upper left), T106 (upper right) and T159 (lower left) forecasts from 12Z, 26 February 1984. An analysis by Shapiro et al. (1987) of aircraft measurements taken at 300 m shortly after this time is shown (for a smaller domain) in the lower right panel.

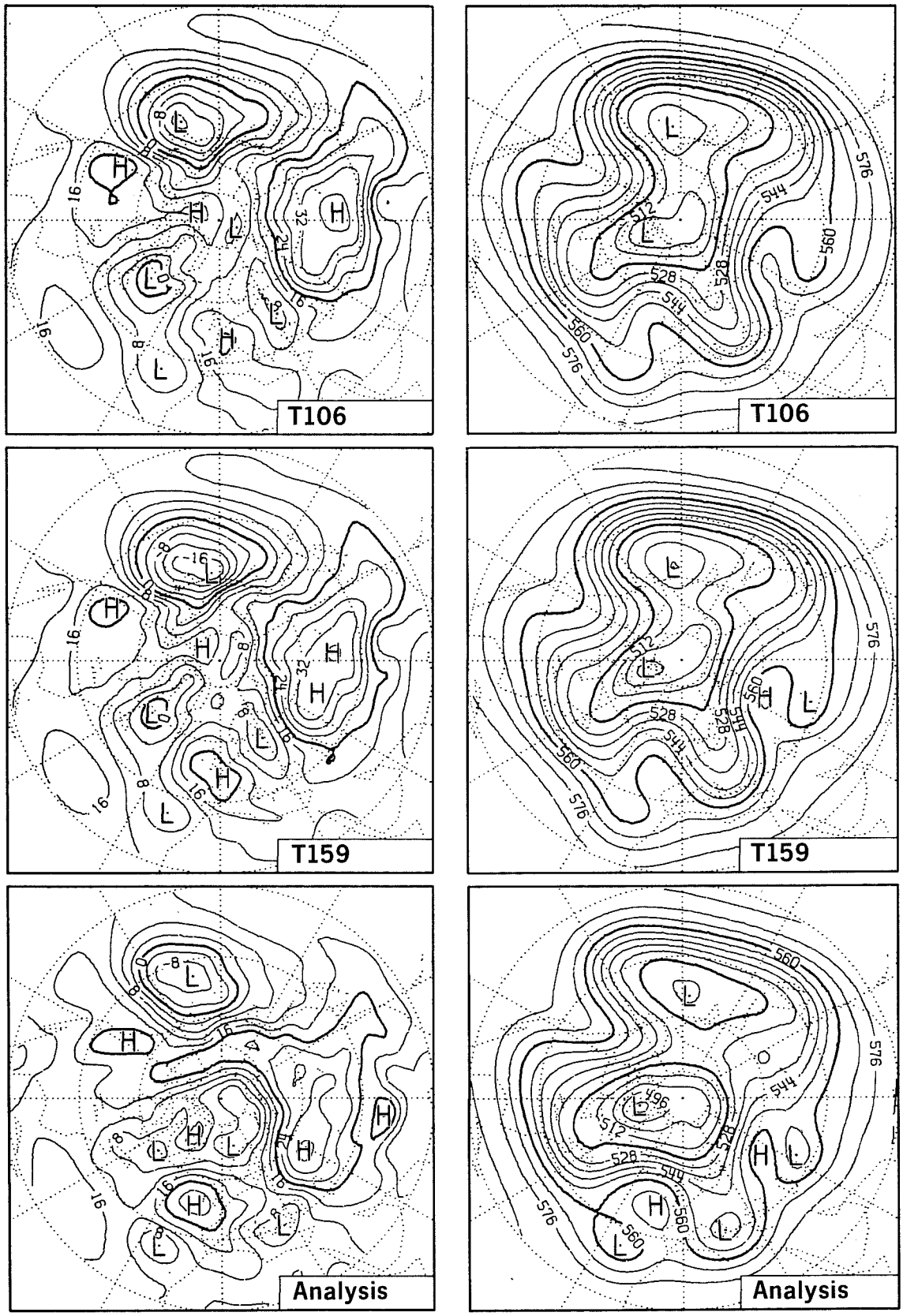

Fig. 23 Mean analyses of 1000 mb (left) and 500 mb (right) height for the period 2-7 March 1984 (lower), and corresponding maps for T106 (upper), and T159 (middle) forecasts from 26 February 1984. Units are dam.

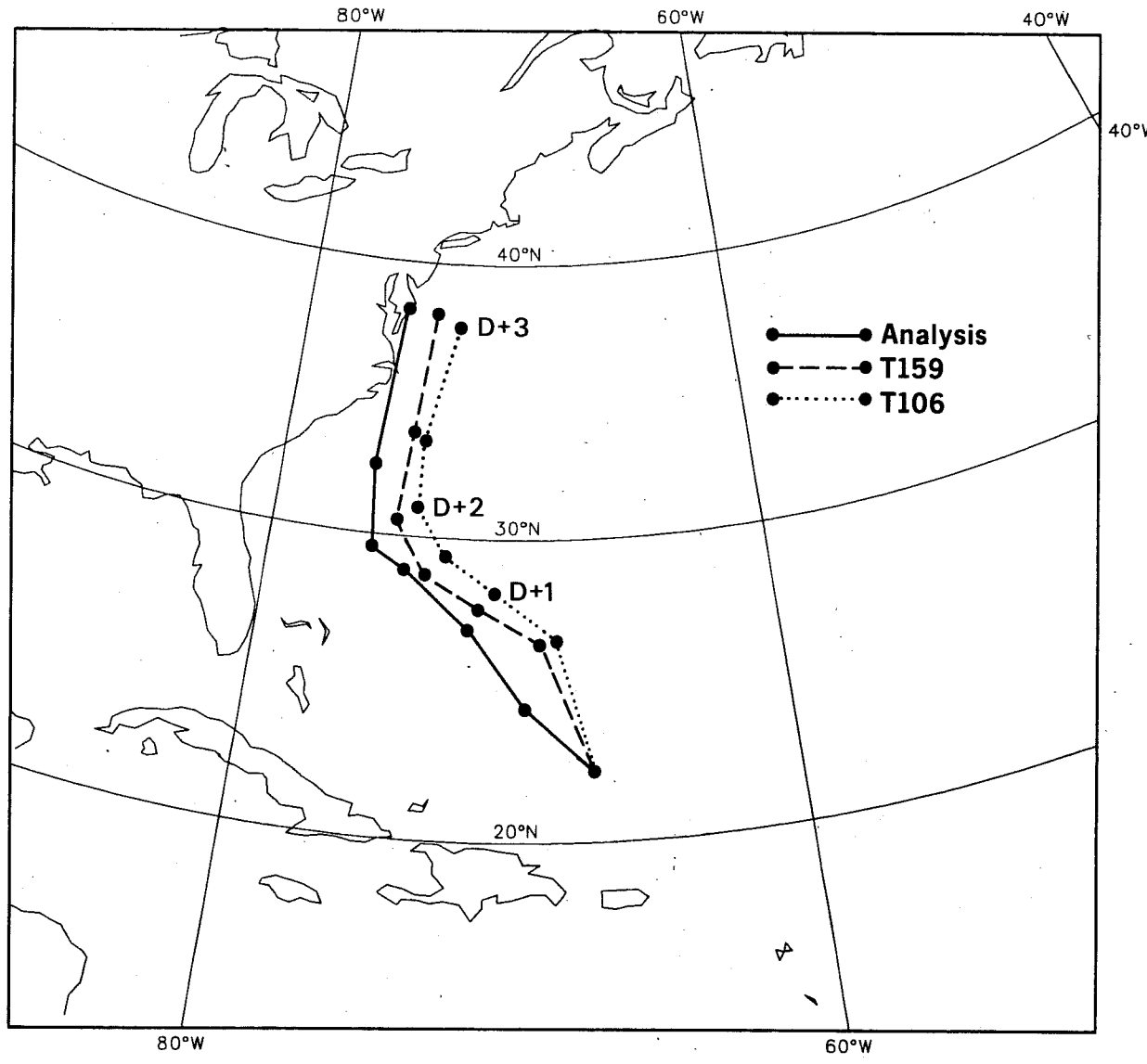

Fig. 24 Tracks of hurricane "Gloria" as analyzed operationally (solid line) for the period 24-27 September 1985, and as forecast from 24 September using T106 (dotted) and T159 (dashed) resolutions.

height and time. The sharpening of thermal structures with increasing resolution is evident, and more rapid spatial changes in wind speed and direction can be discerned for higher resolution. At T159 resolution a warm tongue extends southwestwards from close to the intersection of the Greenwich Meridian and the 70°N latitude, a feature clearly present in reality.

Turning attention from the short to the later medium range, major forecast errors often make it difficult to assess whether forecast changes brought about by increased resolution are truly beneficial, although the case presented earlier in Fig. 12 is an example of a pronounced exception to this rule. The forecast from 26 February 1984, chosen for its short-range interest, was in fact one of relatively high accuracy in the second half of the forecast range, and the differences between T106 and T159 can be directly assessed in comparison with reality. Maps of 1000 and 500 mb height averaged from days 5 to day 10 are compared with corresponding analyses in Fig. 23. Although many of the forecast errors are common to both resolutions, differences in phase and intensity between the forecasts are mostly in favour of T159. Examples are the westward extension of the Siberian high and the anticyclone over western Europe. At 500 mb, the two main centres of the circumpolar vortex located near 75°W and the Dateline are deeper and more realistic in the T159 forecast. A tendency for large eddy amplitudes in higher resolution forecasts was found earlier in the comparison of T63 and T106; it acts to increase forecast accuracy as long as the overall skill of the prediction is high, but tends to bias objective verification towards lower resolution once significant forecast errors have arisen.

(iii) 24 September 1985

The global forecasts in this case were carried out to day 3 to study the evolution of hurricane "Gloria" as it moved towards and then along the eastern seaboard of the USA. The analyzed track of the storm, and the tracks predicted by T106 and T159, are shown in Fig. 24. The better track of the T159 forecast, coupled with a greater (and more realistic) intensity of the system, resulted in a substantial difference in the amount of rainfall forecast over the East Coast. The T106 and T159 predictions for the 12-hour period leading up to 12Z, 27 September, are presented in Fig. 25, which also includes plotted surface weather reports for 12Z on this day. Differences can

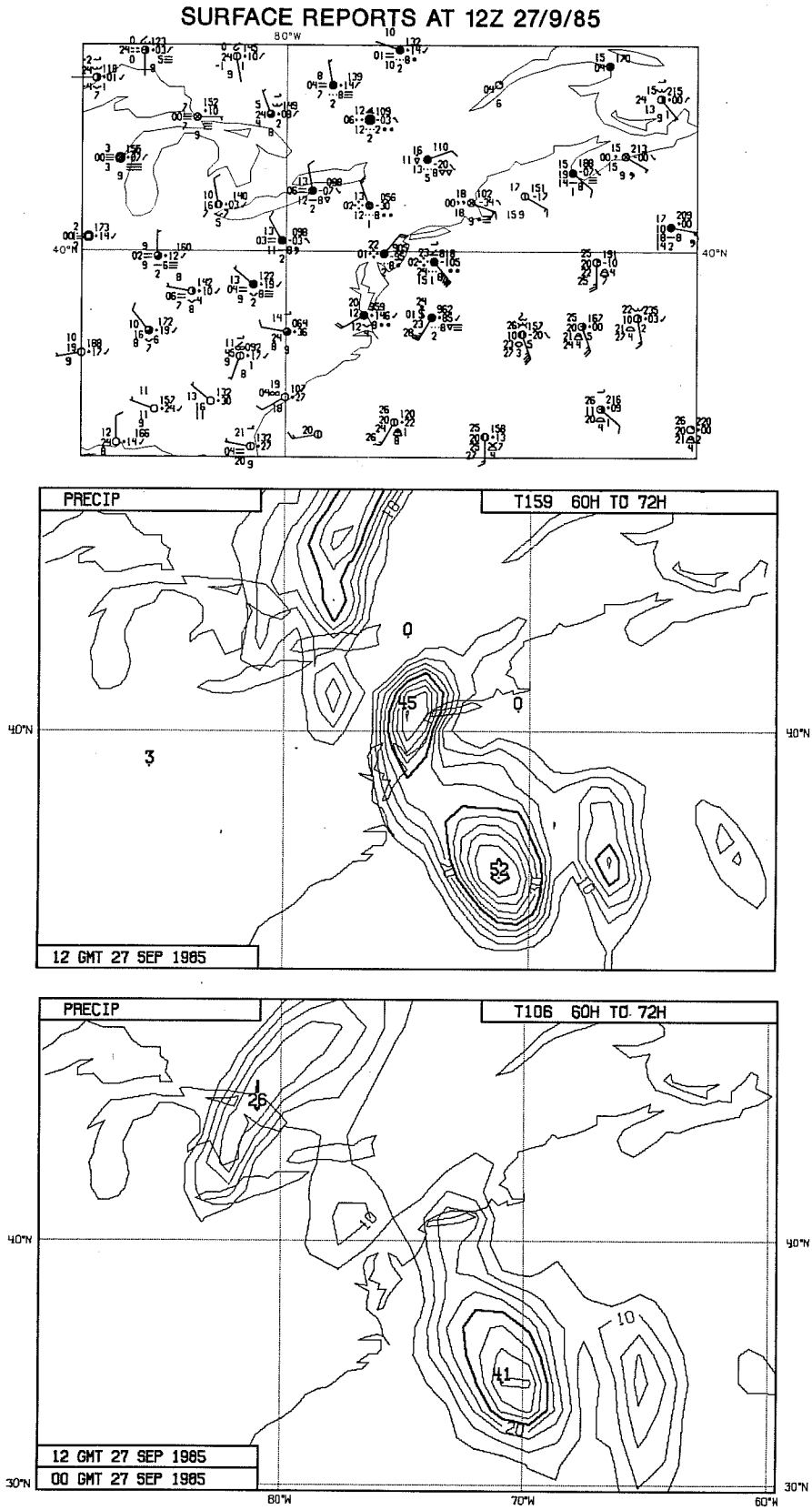

Fig. 25 Surface weather reports at 12Z, 27 September 1985, and precipitation (mm) for the period 00 to 12Z produced by T159 (middle) and T106 (lower) forecasts from 12Z, 24 September.

be seen not only over the East Coast, but also in the precipitation patterns over and to the north of the Great Lakes. Comparison with the surface reports shown in Fig. 25 and those of earlier hours indicates that here also the T159 pattern is the more correct.

(iv) 13 December 1986

The short-range feature of interest in this case is a depression of exceptional depth east of southern Greenland. The T159 forecast in the 36- to 48-hour range gave a low some 5 mb deeper and better positioned than that from T106. Rather than illustrate this (a somewhat similar case has been presented in Fig. 20), we consider a much grosser aspect of model behaviour, and present in Fig. 26 meridional cross-sections of the zonal-mean temperature error averaged from day 5 to 10 for T63, T106 and T159 forecasts. All panels show the tendency of the model to warm the tropical middle and upper troposphere, and to cool at higher latitudes. Consistent with the results on "spin-up" summarized in Fig. 18, the tropical warming increases with increasing resolution.

(v) 15 August 1986

This summer case was chosen because it had already been studied from the viewpoint of the parametrization of convection. The 5-day forecasts with T106 and T159 resolution presented in the left-hand panels of Fig. 27 exhibit only small differences, both failing seriously in their prediction of the development of the low near 20°W and of the eastward movement of the trough downstream of it. This contrasts with a marked sensitivity of this case to the choice of parametrization of convection. In general, higher resolution cannot be expected to compensate for major errors introduced by other parts of the forecasting system.

Examining difference maps for the whole hemisphere for this case revealed the largest differences over northern North America in the second half of the 10-day range. The right-hand panels of Fig. 27 illustrate how the T159 forecast for day 7 captured better the depth and circulation around the low over northwestern Canada and Alaska. Differences in the representations of the cut-off lows to the south can also be seen.

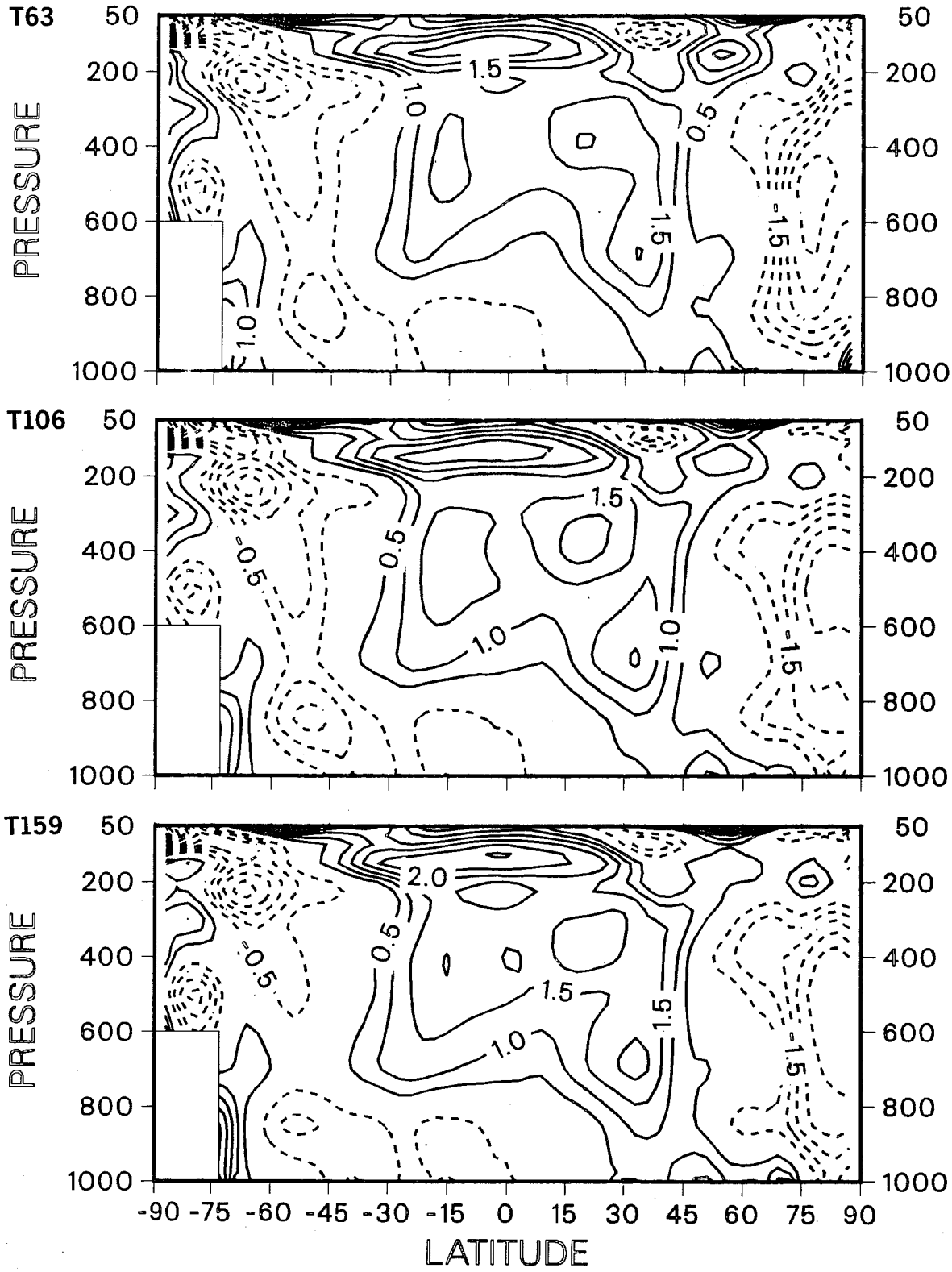

Fig. 26 Cross-sections of the zonal-mean temperature error (contour interval 0.5 K) averaged from days 5 to 10 of T63 (upper), T106 (middle) and T159 (lower) forecasts from 13 December 1986.

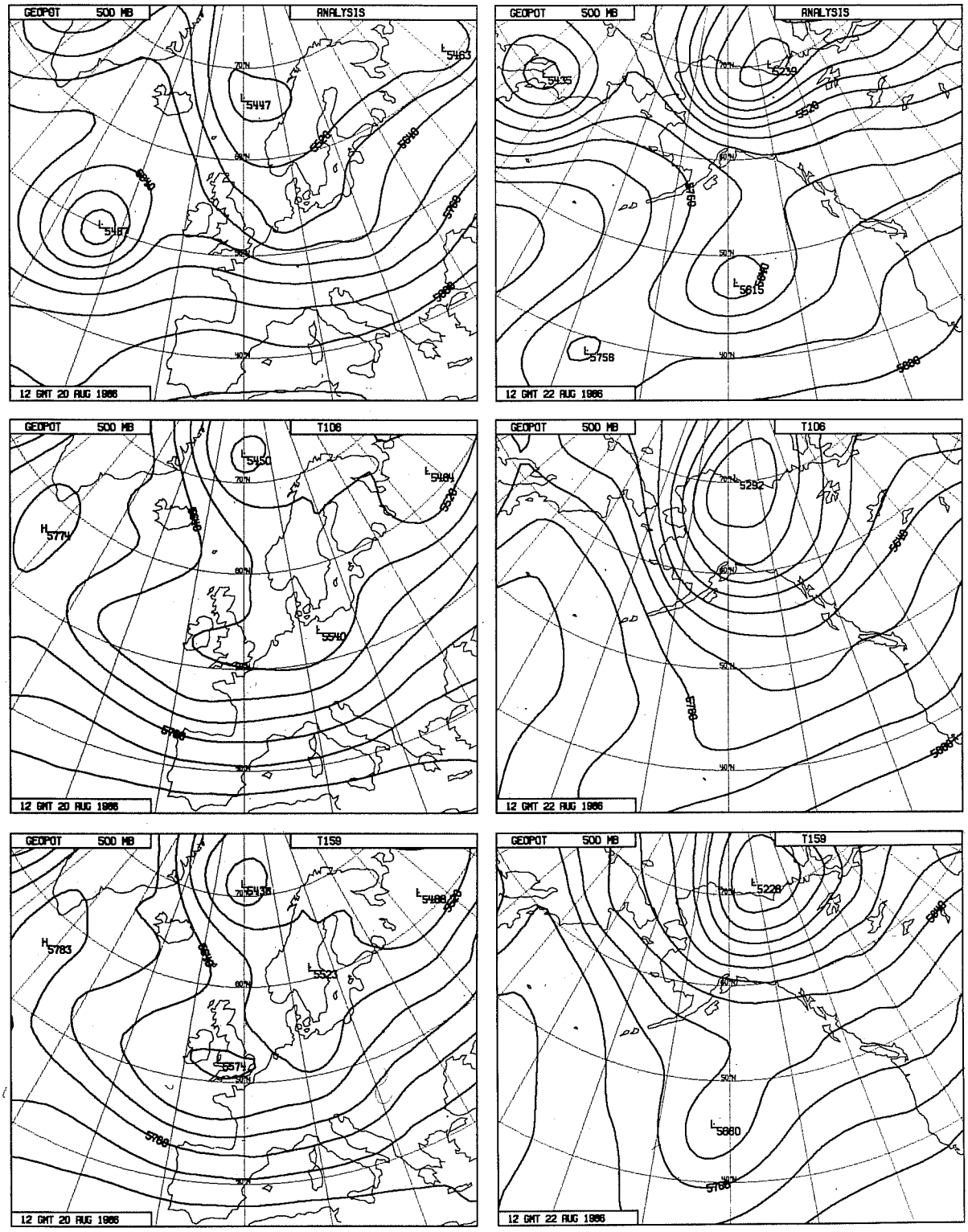

Fig. 27 Analyses of 500 mb height (contour interval 60 dam) for 20 August (upper left) and 22 August (upper right) 1986, and corresponding 5- and 7-day forecasts with T106 (middle) and T159 (lower) resolutions.

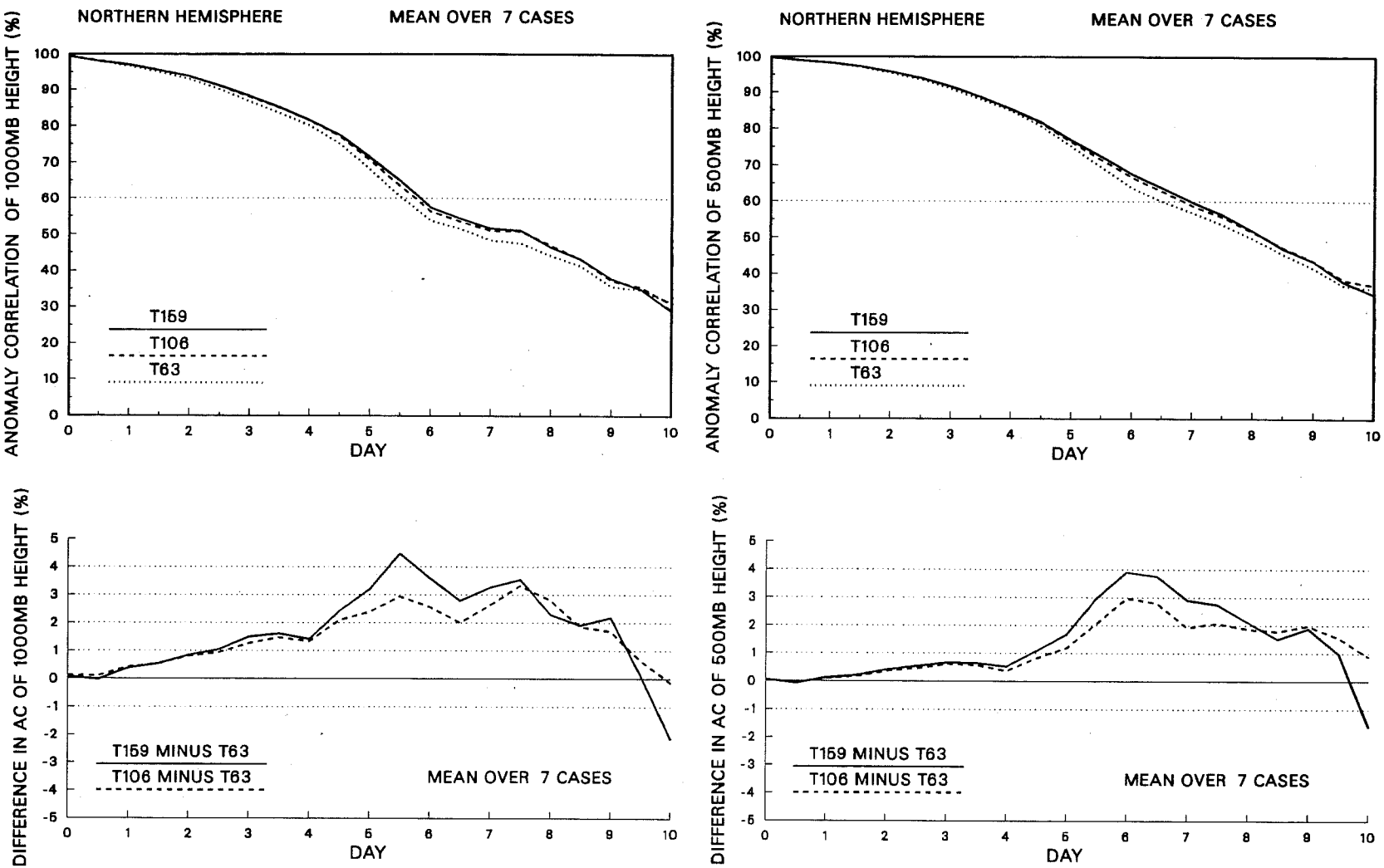

Fig. 28 Mean anomaly correlations of 1000 mb (left) and 500 mb (right) height for forecasts with T159, T106 and T63 resolutions. The upper panels display full values, and differences are shown in the lower plots.

(vi) Objective verification

Overall, 7 T159 forecasts have been carried out to day 10. These, and the corresponding T63 and T106 forecasts, have been verified objectively in the usual way, and mean results for anomaly correlations of the 500 and 1000 mb height fields are shown in Fig. 28. Many qualifying remarks could be made in presenting these results, particularly regarding the absence of high resolution in data assimilation, and the small number of (predominantly winter) cases which may make results rather unrepresentative, especially beyond day 6 or 7. Nevertheless, in the range from day 5 to day 7, T159 improves over T106 by between 30 and 50% of the improvement of T106 over T63, a result broadly consistent with what might have been expected on the basis of extrapolating the results presented for T106 and lower resolutions in Fig. 8.

4. CONCLUDING REMARKS

We have shown how timesteps may be significantly increased in spectral models, at negligible computational cost and with negligible impact on forecast accuracy. Use of a semi-implicit treatment of zonal advection of the vorticity and specific humidity has been found at T63 resolution to enable use of timesteps which are some 25 to 50% longer than would otherwise be possible, and a further 50% increase (from 10 to 15 minutes) can be used safely at T106 resolution (with hybrid vertical coordinate) in conjunction with selectively enhanced horizontal diffusion. Moreover, results have been presented from a set of 10-day T106 forecasts carried out with a timestep of $22\frac{1}{2}$ minutes, corresponding to a gain of a factor of $2\frac{1}{2}$ to 3 in computational efficiency when compared with a standard spectral model with semi-implicit treatment of only the gravity-wave terms. In this case forecast accuracy is impaired later in the forecast range, although conventional objective verification indicates little loss of skill out to 3 or 4 days ahead. At the shorter range there is, however, some indication of noise in situations with strong boundary-layer flow, associated presumably with the time-stepping in the parametrization of vertical diffusion. The stability of the semi-implicit treatment of gravity-wave motion is a further cause for concern when considering use of longer timesteps. These results should be borne in mind as semi-Lagrangian approaches come to be considered for medium-range prediction.

Objective verification of spectral-model forecasts reveals a clear increase in skill as horizontal resolution is refined. Although the mean improvement of T106 over T63 is distinctly smaller than that of T63 over T42, it is nevertheless quite systematic early in the forecast range, particularly at the surface. The impression from subjective synoptic assessment is one of a more decisive advantage of T106 over T63, with quite regular improvements in detail in the first few days of the forecasts, and occasionally substantial impact later in the medium range. More intense and highly structured systems are found at higher resolution, and this tends to bias objective scores towards favouring lower resolution once other sources of error have caused a serious degradation in the synoptic-scale evolution of the forecast. Given a broadly correct prediction of the synoptic pattern, increased horizontal resolution can result in some very clear improvements in local forecasts of weather elements such as precipitation, and low-level wind and temperature. We have also illustrated how some known modelling problems may become more pressing as resolution increases.

Notwithstanding the above comments, the mean differences in skill of T63 and T106 forecasts remain small compared with the large variations in mean skill that are found to occur between one month and another (see, e.g., Simmons 1986), or indeed compared with shorter-term variations in forecast skill. Looking at the future one may foresee the use of higher resolution, vertical as well as horizontal, as providing worthwhile increases in synoptic-scale accuracy and local detail in the first part of the medium range. There may well, however, be a point in the forecast range beyond which increased computational power is better used to run some form of ensemble of forecasts to provide indications of expected reliability. Quite where this point will lie will depend on the extent to which forecasts are improved by the development of better parametrizations and numerical techniques, and by better data assimilation (which itself is somewhat dependent on model resolution), since as other sources of forecast error are reduced, a more pronounced impact of higher resolutions may be anticipated.

References

Asselin, R., 1972: Frequency filter for time integrations. Mon.Wea.Rev., 100, 487-490.

Dell'Osso, 1984: High resolution experiments with the ECMWF model: A case study. Mon.Wea.Rev., 112, 1853-1883.

ECMWF, 1987: Proceedings of 1986 Seminar/Workshop on Observation, theory and modelling of orographic effects. Vol. I. 333 pp.

Jarraud, M., A.J. Simmons and M. Kanamitsu, 1985: Development of the high resolution model. ECMWF Tech.Memo.No.107, 61 pp.

Jarraud, M., A.J. Simmons and M. Kanamitsu, 1988: Sensitivity of medium-range weather forecasts to the use of an envelope orography. To appear in Quart.J.Roy.Met.Soc.

Robert, A. 1981: Stable numerical integration scheme for the primitive meteorological equations. Atmosphere-Ocean, 19, 35-46.

Robert, A.J., J. Hendersen and C. Turnbull, 1972: An implicit time integration scheme for baroclinic models of the atmosphere. Mon.Wea.Rev., 100, p329-335.

Shapiro, M.A., L.S. Fedor and T. Hampel, 1987: Research aircraft measurements of a polar low over the Norwegian Sea. Tellus, 39A, 272-306.

Simmons, A.J., 1986: Numerical prediction: some results from operational forecasting at ECMWF. Advances in Geophysics, Vol. 29, 305-338.

Simmons, A.J., 1987: Orography and the development of the ECMWF forecast model. ECMWF Seminar on Observation, Theory and Modelling or Orographic Effects, 15-19 September, 1987, Reading, U.K., Vol. 2, 129-163.

Simmons, A.J. and D.M. Burridge, 1981: An energy and angular momentum conserving vertical finite difference scheme and hybrid vertical coordinates. Mon.Wea.Rev., 109, 758-766.

Simmons, A.J., D.M. Burridge, M. Jarraud, C. Girard and W. Wergen, 1988: The ECMWF medium-range prediction models. Development of the numerical formulations and the impact of increased resolution. To appear in Meteorology and Atmospheric Physics.

Simmons, A.J., B.J. Hoskins and D.M. Burridge, 1978: Stability of the semi-implicit method of time integration. Mon.Wea.Rev., 106, 405-412.

Simmons, A.J. and M. Jarraud, 1984: The design and performance of the new ECMWF operational model. ECMWF Seminar on Numerical Methods for Weather Prediction, 5-9 September 1983, Reading, U.K., Vol. 2, 113-164.

APPENDIX
Stability Analysis for the Semi-Implicit Treatment of Gravity-Wave Terms

Following the development given by Simmons et al. (1978) for sigma coordinates and Simmons and Burridge (1981) for hybrid coordinates, the divergence, temperature and surface pressure equations for gravity-wave motion are

$$\frac{\partial D}{\partial t} = c_n \left\{ \gamma T' + \delta (\ell n p_s)' \right\} \tag{A.1}$$

$$\frac{\partial T'}{\partial t} = - \tau D \tag{A.2}$$

$$\frac{\partial (\ell n p_s)'}{\partial t} = - \nu . D \tag{A.3}$$

where D and T' are column vectors representing the NLEV values of the (m,n)th spectral component of the divergence and deviation of temperature from the horizontally-uniform temperature of the resting basic state, and $(\ell n p_s)'$ is the (m,n)th component of the deviation of the logarithm of surface pressure from its basic-state value. $c_n = \frac{n(n+1)}{a^2}$, where a is the radius of the earth. γ and τ are NLEV x NLEV matrices and δ and ν are vectors, each depending on the temperatures profile and uniform surface pressure of the basic state. Formulae for computing γ, τ, δ and ν are given by Simmons and Burridge (loc. cit.)

We assume a reference temperature profile and surface pressure leading to reference matrices and vectors γ_r, τ_r, δ_r and ν_r. We test the stability of gravity-wave perturbations to an idealized resting atmospheric characterized by matrices and vectors γ, τ, δ and ν using a semi-implicit time scheme in which terms on the right hand sides of (A.1) - (A.3) which represent gravity-wave perturbations of the reference basic state are computed as the time average $\bar{X} = \frac{1}{2}\beta (X(t+\Delta t) + X(t-\Delta t)) + (1-\beta)X(t)$. β=1 in the usual semi-implicit scheme (Robert et al., 1972). Equations (A.1), (A.2) and (A.3) become

$$\frac{D(t+\Delta t)-D^*(t-\Delta t)}{2\Delta t} = c_n \left\{ \beta \left(\gamma_r \frac{T(t+\Delta t)+T^*(t-\Delta t)}{2} + \delta_r \frac{\ell(t+\Delta t)+\ell^*(t-\Delta t)}{2} \right. \right.$$

$$\left. \left. + (\gamma - \beta \gamma_r) T(t) + (\delta - \beta \delta_r) \ell(t) \right\} \right. \tag{A.4}$$

$$\frac{T(t+\Delta t)-T^*(t-\Delta t)}{2\Delta t} = -\beta\tau_r \frac{D(t+\Delta t)+D^*(t-\Delta t)}{2} - (\tau-\beta\tau_r)\, D(t) \qquad (A.5)$$

$$\frac{\ell(t+\Delta t)-\ell^*(t-\Delta t)}{2\Delta t} = -\beta\nu_r \frac{D(t+\Delta t)+D^*(t-\Delta t)}{2} - (\nu-\beta\nu_r)\, D(t) \qquad (A.6)$$

and we use the time filter (Asselin, 1972):

$$X^*(t) = X(t) + \varepsilon(X(t+\Delta t) + X^*(t-\Delta t) - 2X(t)) \qquad (A.7)$$

for X=D, T and ℓ. Here we have dropped primes and replaced ℓnp_s by ℓ. The values $\beta = 0.75$ and $\varepsilon = 0.1$ are currently used operationally at ECMWF.

We look for modes with amplification factor λ:

$$X(t+\Delta t) = \lambda\, X(t) \qquad (A.8)$$

(A.7) gives

$$(\lambda-\varepsilon)\, X^*(t-\Delta t) = ((1-2\varepsilon)\ \lambda + \varepsilon\lambda^2)\, X(t-\Delta t) \qquad (A.9)$$

Substituting (A.8) and (A.9) into (A.4), (A.5) and (A.6) gives

$$(\lambda^2(\lambda-\varepsilon) - (\varepsilon\lambda^2+(1-2\varepsilon)\lambda))D(t-\Delta t)$$

$$= c_n \Delta t \left\{(\lambda^2(\lambda-\varepsilon) + \varepsilon\lambda^2 + (1-2\varepsilon)\lambda)\ \beta\ (\gamma_r T(t-\Delta t)+\delta_r \ell(t-\Delta t)\right.$$

$$\left. +2\lambda(\lambda-\varepsilon)\ ((\gamma-\beta\gamma_r)T(t-\Delta t)+(\delta-\beta\delta_r)\,\ell(t-\Delta t))\right\} \qquad (A.10)$$

$$(\lambda^2(\lambda-\varepsilon) - (\varepsilon\lambda^2+(1-2\varepsilon)\lambda))T(t-\Delta t)$$

$$= -\left\{(\lambda^2(\lambda-\varepsilon) + \varepsilon\lambda^2 + (1-2\varepsilon)\lambda)\ \beta\ \tau_r D(t-\Delta t)\right.$$

$$\left. +2\lambda(\lambda-\varepsilon)\ (\tau-\beta\tau_r)D(t-\Delta t)\right\} \qquad (A.11)$$

$$(\lambda^2(\lambda-\varepsilon) - (\varepsilon\lambda^2+(1-2\varepsilon)\lambda))\,\ell(t-\Delta t)$$

$$= -\left\{(\lambda^2(\lambda-\varepsilon) + \varepsilon\lambda^2 + (1-2\varepsilon)\lambda)\ \beta\ \nu_r D(t-\Delta t)\right.$$

$$\left. +\lambda(\lambda-\varepsilon)\ (\nu-\beta\nu_r)D(t-\Delta t)\right\} \qquad (A.12)$$

Eliminating $T(t-\Delta t)$ and $\ell(t-\Delta t)$ we obtain

$$(\lambda^2-2\varepsilon\lambda-1+2\varepsilon)^2 D + c_n \Delta t^2 \{(\lambda^2+1-2\varepsilon)^2 B_r + 4(\lambda-\varepsilon)^2 B_e + 2(\lambda^2+1-2\varepsilon)(\lambda-\varepsilon) B_x\} D = 0 \quad (A.13)$$

where $B_r = \beta^2(\gamma_r \tau_r + \delta_r \nu_r)$ (A.14)

$$B_e = (\gamma-\beta\gamma_r)(\tau-\beta\tau_r) + (\delta-\beta\delta_r)(\nu-\beta\nu_r) \quad (A.15)$$

$$B_x = \gamma_r(\tau-\beta\tau_r) + (\gamma-\beta\gamma_r)\tau_r + \delta_r(\nu-\beta\nu_r) + (\delta-\beta\delta_r)\nu_r \quad (A.16)$$

(A.13) can be written

$$(\lambda^4 I - \lambda^3 M_1 - \lambda^2 M_2 - \lambda M_3 - M_4) D = 0 \quad (A.17)$$

where I is the unit matrix, and

$$M_1 = (B_r + \frac{1}{c_n \Delta t^2} I)^{-1} (\frac{4\varepsilon}{c_n \Delta t^2} I - 2 B_x)$$

$$M_2 = (B_r + \frac{1}{c_n \Delta t^2} I)^{-1} (\frac{2(1-2\varepsilon(1+\varepsilon))}{c_n \Delta t^2} I + 2\varepsilon B_x - 4 B_e - 2(1-2\varepsilon) B_r)$$

$$M_3 = (B_r + \frac{1}{c_n \Delta t^2} I)^{-1} (\frac{4\varepsilon(2\varepsilon-1)}{c_n \Delta t^2} I + 8 \varepsilon B_e - 2 (1-2\varepsilon) B_x)$$

$$M_4 = (B_r + \frac{1}{c_n \Delta t^2} I)^{-1} (- \frac{(1-2\varepsilon)^2}{c_n \Delta t^2} I - (1-2\varepsilon)^2 B_r - 4\varepsilon^2 B_e + 2\varepsilon(1-2\varepsilon) B_x)$$

λ is thus an eigenvalue of the 4NLEV x 4NLEV matrix

$$\begin{matrix} 0 & I & 0 & 0 \\ 0 & 0 & I & O \\ 0 & 0 & 0 & I \\ M_4 & M_3 & M_2 & M_1 \end{matrix}$$

An eigenvalue with modulus greater than 1 implies instability of the semi-implicit time scheme. The eigenvectors of the above matrix take the special form

$$D$$
$$\lambda D$$
$$\lambda^2 D$$
$$\lambda^3 D$$

where the column vector D of dimension NLEV is the divergence structure of the mode.

A number of stability analyses have been carried out for various combinations of model parameters, reference and actual states. An example of dependence on the values of β and ε and on the reference and actual surface pressures is shown in Table A.1. The caption provides further details of the calculations. For the operational choices of 800 mb for the reference pressure and ε=.1, differences between the stability of the scheme with β=1 and that with β=0.75 appear to be very small. It should be noted, however, that the stabilizing influence of the time filter is more pronounced for the smaller value of β.

Surface Pressure (mb)		β=1	β=.75	β=1	β=.75
Actual	Reference	ε=.1	ε=.1	ε=.01	ε=.01
1013.2	1013.2	St	St	St	St
750	1013.2	St	St	24	20
500	1013.2	15	14	9	3
1013.2	800	St	St	St	St
750	800	St	St	St	St
500	800	26	25	14	10
1013.2	500	St	22	St	3
750	500	St	56	St	St
500	500	St	St	St	St

Table A.1